X-611-68-6
PREPRIN



# OBSERVATIONS OF TRAPPED ELECTRONS AT LOW AND HIGH ALTITUDES





D. J. WILLIAMS
J. F. ARENS
L. J. LANZEROTTI



FEBRUARY 1968

GODDARD SPACE FLIGHT CENTER
GREENBELT, MARYLAND

ENERGETIC PARTICLES BRANCH

# PRECIPITATION OF TRAPPED ELECTRONS AT LOW AND HIGH ALTITUDES

by

R. A. Williams, J. F. Arens*
Goddard Space Flight Center
Greenbelt, Maryland 20771

and

L. J. Lanzerotti
Bell Telephone Laboratories, Incorporated
Murray Hill, New Jersey 07974

*NASA-NAS Postdoctoral Resident Research Associate

ABSTRACT

Simultaneous trapped electron data have been obtained for near equatorially mirroring electrons by the Explorer 26 satellite and for low altitude mirroring electrons by the satellite 1963 38C. Electron energies $\geq$300 keV, $\geq$450 keV, and $\geq$1.0 MeV were sampled by the Explorer 26 instrumentation and $\geq$280 keV and $\geq$1.2 MeV by the 1963 38C instrumentation. These data are presented for the time period January 1 through June 29, 1965, for L = 3.0, 3.5, 4.0, 4.5, 5.0, and 5.5. The data and subsequent analyses indicate that (1) $\gtrsim$300 keV electrons rapidly ($\lesssim$0.1 day) reach an equilibrium distribution within a flux tube after a large magnetic disturbance thereby causing long term (many day) cross-L diffusion and decay effects to appear pitch angle independent at these energies; (2) these same effects display a strong pitch angle dependence for $\gtrsim$ 1 MeV electrons due to the longer time required for these higher energy electrons to attain an equilibrium distribution within a given flux tube; (3) this difference between the ~300 keV and ~1 MeV electron behavior can be due to a decreased effectiveness of pitch angle scattering mechanisms in lowering the mirror points of the higher energy electrons - e.g., assuming interaction with wide band whistler mode noise (Roberts, 1968 ) as the major scattering mechanism, the power spectral density function

would have to significantly decrease in magnitude at frequencies lower than a few hundred cycles per second; (4) the intensities of both low and high altitude trapped $\gtrsim$ 300 keV electrons exhibit a fast decay mode immediately after the April 18, 1965, magnetic storm and a significantly slower decay several days after the storm, in the region of maximum disturbance, L ~ 3.0; (5) a comparison of particle response characteristics at low and high altitudes during a main phase storm yields a rough measure of field expansion in the storm - expansions of $\Delta R \gtrsim 0.2\ R_E$ at $R \sim 5.5\ R_E$ for a maximum negative Dst of -30$\gamma$ and $\Delta R \sim 0.5\ R_E$ at $R \sim 3.2\ R_E$ for $Dst^{max} = -137\gamma$ are obtained; (6) energetic electrons associated with magnetic storms are observed to initially appear at L values well within the trapping regions and subsequently diffuse to lower and higher altitudes; (7) preliminary results indicate that the acceleration mechanisms responsible for the appearance of energetic electrons within the trapping regions during main phase storms act on the high altitude side of the whistler knee and may be responsible for the observed apparent motion of the whistler knee to lower altitudes during magnetic storms (Carpenter, 1966); (8) the appearance of energetic electrons in the trapping regions from the equator to low altitudes during the April 17, 1965, storm correlates very well spatially with an observed depletion of maximum ionospheric electron density, Nm F2 (Bauer and Krishnamurthy, 1967).

## INTRODUCTION

There have been a number of experimental studies reported concerning the behavior of energetic outer zone electrons at high altitudes (see for example Freeman, 1964, Frank, 1965a) and at low altitudes (see for example, Forbush et al., 1962; O'Brien, 1963, 1964; Rose, 1966; Williams, 1966). Such studies have contributed to our understanding of the electron spatial distributions and their relation to the distorted geomagnetic field and to the time behavior of these particles and its relation to magnetic activity.

As these results emerged, efforts have turned toward studying possible source, loss, and transport mechanisms responsible for the observed trapped particle behavior (e.g., Nakada and Mead, 1965; Roberts, 1966; Kennel and Petschek, 1966; Tverskoy, 1964; Falthammer, 1965). In general, simultaneous observations from several locations within the magnetosphere are required to determine the problems and obtain possible solutions.

Therefore, in an effort to obtain further information concerning these mechanisms, we present herein a comparison of the time behavior of electrons mirroring near the magnetic equator and those mirroring at low altitudes. Energies $\gtrsim$280 keV and $\gtrsim$1 MeV are considered over the L range $3 < L < 5.5$. The data were obtained from the low inclination, high altitude

satellite Explorer 26 and the low altitude polar orbiting satellite 1963 38C over the time period January 1, 1965, through June 29, 1965. Preliminary results, covering only the April 17, 1965, magnetic storm were reported by Arens et al. (1967).

While such an approach is far from ideal, it does offer the opportunity of obtaining a further insight into these various mechanisms by observing the simultaneous behavior of particles trapped near the equator and at the end of the field line.

## SATELLITES, INSTRUMENTATION, AND ORBITS

The Explorer 26 satellite was launched on December 21, 1964 into an orbit having an inclination of 20.1°, an orbital period of ~7.5 hours, an apogee of 26,000 km, and a perigee of 200 km. The satellite was spin oriented with the angle between the spin vector and the local magnetic field ranging from about 30° to 90°. The satellite spin rate gradually and uniformly slowed from about 32 rpm to about 9 rpm during the period discussed in this paper.

The experiment flown by BTL on Explorer 26 was designed to investigate the electron and proton particle populations in the trapped radiation belts. The experiment consisted of six solid state partially depleted p-n junction detectors (Buck et al. 1964). By making use of the electron and proton energy loss characteristics and by changing the thickness of the detector active region by a change in detector bias, it was possible to distinguish between proton and electron responses in the data. The detectors were encapsulated in a nitrogen-oxygen mixture at atmospheric pressure and covered by a 0.3 mil Kovar diaphram. Additional absorbers were used in individual detectors to allow the detection of a wide range of particle energies.

The three Explorer 26 detectors whose electron flux observations are discussed in this paper were designated E5, E6, and E1 and had electron threshold energies of 0.3 MeV,

0.45 MeV, and 1.0 MeV, respectively. The E5 and E6 detectors were directional, had look angles oriented normal to the satellite spin axis, and were operated in the high bias, or electron mode. The E1 detector was omni-directional, its symmetry axis oriented perpendicular to the satellite spin axis, and was also operated in the high bias mode. The efficiency-geometrical factors for E5, E6, and E1 were $1.5 \cdot 10^{-3}$ cm$^2$ ster, $4.0 \cdot 10^{-3}$ cm$^2$ ster, and $3.0 \cdot 10^{-3}$ cm$^2$ ster, respectively.

A comparison of the high bias mode with the low bias mode of the experiment showed that at L = 4.5, 5.0, and 5.5, there was essentially no contamination of the electron data from protons. At L = 3.0, 3.5, and 4.0 the high bias data consisted of an admixture of electrons and protons except for the times when the fluxes were increased by magnetic storms. At this time, the high bias-low bias comparison indicated that the increased fluxes were essentially all electrons.

Satellite 1963 38 was launched on September 28, 1963 into nearly circular polar orbit having a 1147 km apogee, a 1067 km perigee, a 89.9° inclination and a 107.4 minute period. The detectors of interest on 1963 38C are two 1000 micron surface barrier solid state detectors measuring integral electron intensities at $E_e \geq 280$ keV and $\geq 1.9$ MeV. As the satellite is magnetically aligned and the detectors are

oriented to look out normal to the alignment axis, trapped electron intensities are obtained for those electrons mirroring at or very near the point of observation. Further details concerning the satellite and instrumentation have been reported by Williams and Smith (1965).

During the time period being considered here, January 1, 1965, through June 29, 1965, the apogee of Explorer 26 precessed through the local time interval of 1630 hours to 1117 hours. Similarly, the orientation of the orbital plane of 1963 38C with respect to the earth-sun line swept through all local times. This is illustrated in Fig. 1 where the projection of the two orbits onto the ecliptic plane is shown as viewed looking down from above the north pole.

## DATA

Trapped electron intensities were monitored simultaneously by the satellites Explorer 26 and 1963 38C throughout the period January 1, 1965, through June 29, 1965. The electron energies sampled were $E_e \geq 280$ keV and $\geq 1.0$ MeV aboard 1963 38C and $E_e \geq 300$ keV, $\geq 450$ keV, and $\geq 1.0$ MeV aboard Explorer 26.

Electron intensities through the outer zone were obtained from the 1963 38C data by constructing five point averages at all desired L shells. This process yields an L spread of ±0.04 at L = 3 and ±0.1 at L = 5.5. The response of an on board proton spectrometer has shown that proton contamination in these low altitude high latitude regions is negligible (Williams and Smith, 1965; Williams, 1966).

In the following data presentation, each data point from the Explorer 26 satellite corresponds to the median counting rate observed by one of the electron detectors as the satellite made one pass through the region of space defined by $L \pm 0.05\ R_E$. The data points correspond to $B_o/B$ values ranging from about 0.3 to 1.0. Plots of the counting rate versus $B_o/B$ for L = 4.5, 5.0, and 5.5, indicate that the electron rates generally are essentially independent of $B_o/B$ within the observed range. Where this is not true, L = 3.0, 3.5, and 4.0, the electron data have all been normalized to the rates of $B_o/B = 1$.

The digital accumulation time for one of the Explorer 26 detectors in its electron mode was 1.43 seconds. Due to the spin rate of the satellite, the data from E5 and E6 that is presented in the next section is thus the spin-averaged electron flux from a directional detector. Most of the E5 and E6 data points correspond to data taken with the satellite spin axis at an angle of greater than 60° to the local magnetic field. Thus the spin averaged directional flux from Day 1 to about Day 120, 1965, is equivalent to the omnidirectional flux to within a factor of 1.5. After approximately Day 120, 1965, the spin rate of the satellite had slowed sufficiently so that the experiment sampled less than 180° in the 1.43 second counting interval. An examination of the individual data points at each L value revealed that the effect of the slowing spin was observed mainly in the proton background at L = 3.0 and 3.5. The broad electron pitch angle distributions obscured any noticeable spin modulation in the electron fluxes. No corrections to the data were necessary for this spin effect.

All the data for the period of interest from the $\geq$ 300 keV channel aboard Explorer 26 and the $\geq$ 280 keV channel aboard 1963 38C are shown in Figure 2 for the shells L = 3.0, 3.5, 4.0, 4.5, 5.0, and 5.5. Included in the figure are plots of Dst (Sugiura and Heinrichs, personal communication) and

Kp along with a measure of the orientation of the orbital plane of 1963 38C as viewed from above the north pole. Figure 3 is a similar plot for the data from the Explorer 26 $\geq$ 1.0 MeV channel and the 1963 38C $\geq$1.2 MeV channel.

Table 1 lists the conversion factors required to convert the relative counts shown in Figures 2 and 3 to absolute flux values (particles/$cm^2$ster sec). The errors shown are mainly due to spectral uncertainties.

TABLE I

Conversion Factors for Flux Values

| Channel | Multiply counts by ($cm^{-2}$ster$^{-1}$ sec$^{-1}$) | Error |
|---|---|---|
| 1963 38C $\geq$280 keV | 600 | ±100 |
| 1963 38C $\geq$1.2 MeV | 1200 | ±400 |
| Explorer 26 $\geq$300 keV | 900 | ±300 |
| Explorer 26 $\geq$1.0 MeV | 1200 | ±400 |

The proton sensitivity of the Explorer 26 $\geq$ 300 keV channel can be seen in Figure 2 to extend out to L = 4.0. However, the general features of the trapped electron storm time behavior can be observed and compared with the low altitude data.

A feature of interest shown by Figures 2 and 3 is the significant increase in the detailed response of outer zone trapped electrons to magnetic activity as L increases. At L = 3, only large, well defined perturbations in the magnetic activity indices are associated with intensity changes in the trapped electron population. With increasing L, more and more intensity fluctuations appear which can be associated with a variety of magnetic perturbations. Finally at L = 5.5 shown in Figures 2 and 3, intensity fluctuations appear which have no obvious association with a Dst variation. This lack of association is not surprising since the high L shells are well removed from the near equatorial stations used to determine the Dst values. However, it does emphasize the trend that the trapped electron sensitivity to magnetic activity increases significantly with increasing L, in agreement with previous 1963 38C results (Williams and Smith, 1965; Arens and Williams, 1967).

Figures 2 and 3 also show that the behavior of electrons mirroring near the equator and at low altitudes is very similar, particularly at ~300 keV. Perturbations in the ≥300 keV electron intensities at a given L value are observed generally to come quickly to equilibrium. This causes the electron population to behave in unison throughout a flux tube over extended periods of time. The important distinction between identical low and high altitude L values (Figures 2 and 3) and a flux tube (line of force) is discussed in later sections of this paper.

Exceptions to the above uniform behavior occur near the beginning of magnetic storms with the appearance of electrons new to these regions of observation. It also appears that the relative behavior of equatorially mirroring and low altitude mirroring $\gtrsim$ 1 MeV electrons differs from that at ~300 keV.

To illustrate these differences, Figures 4 and 5 show on an expanded time scale several days of data taken around the geomagnetic storms of March 2, 1965 and June 15, 1965. Included in the plots are AE indices (Fairfield, personal communication) along with the Dst values.

First it is noted that all along the field line the $\gtrsim$300 keV electrons rise to their maximum values much faster than do the $\gtrsim$1 MeV electrons. This was observed to hold for all the major storms in the period under consideration in agreement with earlier results (e.g., Freeman, 1964, and Williams and Smith, 1965).

Secondly it appears that the $\gtrsim$300 keV electrons reach equilibrium within a given flux tube faster than do the $\gtrsim$1 MeV electrons. In Figures 4 and 5 it can be seen that the low altitude trapped electron intensities at $\geq$280 keV reach their peak value soon after the equatorial intensities and then essentially follow the behavior of the equatorial electron population. In fact, increases in the equatorial to low

altitude intensity ratio are observed to occur only during the 1-3 day period associated with the storm main phase depression for the $\gtrsim$280 keV population. At these times field expansion effects invalidate the concept of both low and high altitude L values characterizing the same line of force.

It can further be seen in Figures 4 and 5 that a similar relative behavior between equatorially mirroring and low altitude mirroring electrons is not observed at $\gtrsim$1 MeV. Not only do the low altitude $\gtrsim$1 MeV trapped electron intensities generally reach peak values well after the equatorial intensities, but in several instances continue to increase in intensity long after the equatorial intensities have begun their decay (e.g., L = 4.5, Figure 4, L = 5.0, Figure 5). In addition, variations in the equatorial to low altitude intensity ratio are observed to generally last for several days beyond the main phase depression. Thus, the time to attain equilibrium along a given L shell appears significantly longer at $\gtrsim$1 MeV than at $\gtrsim$300 keV. Note however an apparent change in this pattern at L = 5.5 in Figure 5.

A detailed study of the data in Figures 2 and 3 reveals a wide variety of electron intensity fluctuations which may be associated with various geomagnetic perturbations. In this paper we have chosen to study events characterized by large intensity increases occurring throughout the region

of observation which could be associated with a well defined magnetic storm. This study will thus emphasize the non-adiabatic appearance of new particles in the region of observation and the subsequent behavior of these particles.

The storms studied are indicated by the arrows in Figures 1 and 2 and are listed in Table 2. The Dst zero crossing time is the time at which the Dst values cross and remain below the zero level as the initial phase of the storm begins.

TABLE 2

Major Storms Studied in Period January 1 - June 29 1965

| DATE | SC | MAXIMUM Dst (GAMMA) | Dst ZERO CROSSING TIME |
|---|---|---|---|
| Feb. 6 | 1414 hrs | - 55 | 0130 hrs Feb. 7 |
| Mar. 2 | 1349-1458 hrs <10 stations reported SC | - 68 | 1700 hrs Mar. 3 |
| Mar. 22 | NONE | - 31 | 0330 hrs Mar. 23 |
| April 17 | 1313 hrs | -137 | 0330 hrs April 18 |
| June 15 | 1100 hrs | -102 | 0400 hrs June 16 |

An important parameter in characterizing the outer zone electron response to major magnetic perturbations is the arrival time of the bulk of new particles within a flux tube. The accurate determination of the start of the particle increase associated with the initial phase of the storm is complicated by several factors: (i) adiabatic effects due to sudden commencement compressions and ring current decompressions of the magnetosphere prior to and during the development of the storm; (ii) the appearance of particles associated with polar substorm events which may not be associated with the large bulk increases of electron intensities during the storm main phase; (iii) the measurement of relative arrival times of particles on various L shells by an individual satellite has a resolution governed by the satellite's orbital motion and; (iv) the fact that all of the preceeding effects have strong spatial variations.

In an attempt to minimize these difficulties, we have used the time for the electron intensity increases to reach one half of their maximum value, $t_{m/2}$, as a measure of the arrival time on a given L shell of energetic electrons associated with a main phase geomagnetic storm. Generally, (see Figure 1) the larger intensity increases are rapid enough so that $t_{m/2}$ is quite insensitive to the above effects. The time for the observed intensity increases to attain full peak values on a given L shell was not used as a characteristic

arrival time because it is very sensitive to diffusion effects and is therefore significantly less accurate than $t_{m/2}$. However, while the time of maximum may frequently be very difficult to obtain, the intensity at maximum can be measured quite accurately, thus allowing a determination of $t_{m/2}$ to an accuracy not realizable in finding the time of maximum.

Some of these various problems are illustrated by the data in Figures 6 and 7. Figure 6 shows a sequence of low altitude outer zone profiles along with Dst and AE plots just prior to and during the initial phase of the February 5, 1965 magnetic storm. Pass 1, occurring close to the sudden commencement, displays no noticeable effects, and is shown for orientation purposes. Pass 2 is closely associated with the occurrence of a polar substorm as indicated by the spike in the AE indices and shows an intensity enhancement at high latitudes. Simultaneous data obtained from the 1963 38C proton spectrometer show that this enhancement was due to electrons only (Bostrom et al., 1967). Passes 3 and 4, obtained at the start of the initial phase, show the subsequent loss of these high latitude electrons. Such a loss may be explained by a combination of adiabatic effects and loss from the trapping regions. Pass 5 shows the appearance of large numbers of trapped $\geq$280 keV electrons on the lower L shells.

Pass 6 obtained at the recovery of Dst to approximately prestorm values shows the additional appearance of electrons at $5 \leq L \leq 9$. This may be the combined result of electrons injected at low L shells diffusing outward and electrons injected near the equator diffusing down the field line to these low altitudes.

It is seen from Figure 6 that the bulk of the electrons associated with this main phase storm appear between passes 4 and 5. The appearance of particles on high L shells during pass 2 which are associated with a polar substorm would yield a false start time for the bulk of the particles associated with the main phase Dst decrease. The use of $t_{n/2}$ avoids the above difficulty.

Figure 7 again shows the February 5, 1965 storm but from the perspective of a time history of the comparison between the high altitude and low altitude data. Explorer 26 and 1963 38C data are shown for $E_e \gtrsim 300$ keV for L = 4.0 and 5.0. Dst and AE values are also included. The Explorer 26 data show the appearance of electrons at L = 5.0 occurring significantly before L = 4.0 (Lanzerotti, 1968). However, the above arguments indicate that the two Explorer 26 points after the sudden communcement at L = 5.0 may be associated with the polar substorm occurring at that time and before the start of

the storm main phase. The 1963 38C data shown at L = 5.0 also display an increase at this time but the following data point at the beginning of the storm initial phase shows the decrease discussed in Figure 6 above. It is possible that the Explorer 26 observations at L = 5.0 simply missed this decrease due to sampling resolution. The rapid rise and the magnitude of the main electron intensity increase indicates again that $t_{m/2}$ is not very sensitive to the above effects.

Thus, from the above arguments we feel that $t_{m/2}$ is a more accurate measure of the characteristic time of arrival of energetic particles associated with a main phase geomagnetic storm than either the start of an intensity increase or the time to the maximum increase.

## RESULTS

Figures 8-12 show plots of $t_{m/2}$ as a function of L value for low altitude mirroring electrons ($E_e \geq 280$ keV and $\geq 1.2$ MeV) and near-equatorially mirroring electrons ($E_e \geq 300$ keV and $\geq 1.0$ MeV) for the five magnetic storms being studied. Also shown in Figures 8-12 are the maximum intensities attained during the respective storms for the various energies and altitudes observed.

These data show that there tends to exist for both the low altitude and high altitude data, a range of L values which is associated with both a minimum in $t_{m/2}$ and a maximum in the number of newly observed electrons (see in particular Figures 11 and 12). This indicates that energetic electrons may appear during a main phase geomagnetic storm well within the stable trapping regions and subsequently diffuse both in toward lower L shells and out toward higher L shells. This observation is significant as it shows that the source of these outer zone electrons is not necessarily the diffusion inward of a low energy electron population located at the outer edge of the stable trapping region. In fact, a distant lower energy electron population will result from the outward diffusion of an energetic electron population appearing initially at low L shells. Before discussing our interpretation of the significance of these results, we shall discuss in detail the electron data for each of the storms under consideration.

February 6, 1965

The data from this storm are presented in Figure 8. The maximum intensities observed at 1100 km occurred at $L \simeq 4.5$ for both the $\geq$280 keV and $\geq$1.2 MeV electrons. The equatorial electrons show a maximum intensity at $L \simeq 4.5$ at $\geq$1.0 MeV and $L \simeq 4.5$-5.0 at $\geq$300 keV.

The data for $t_{m/2}$ are not as clear. The 1100 km data indicate a minimum at $L \simeq 4.5$ at $\geq$1.2 MeV and a broad minimum from $L \simeq 3.5$-5.5 for the $\geq$280 keV electrons. While the $\geq$280 keV data may be fit with a curve yielding a minimum $t_{m/2}$ consistent with the $\geq$1.2 MeV data, the difference in the width of the curves may be due to the source being sufficiently strong only at $L \simeq 4.5$ to produce a significant number of $\geq$1.2 MeV electrons.

The equatorial data points for $t_{m/2}$ indicate that both $\geq$300 keV and $\geq$1.0 MeV electrons initially arrive beyond the region of observation, i.e., $L > 5.0$. Note that the lower energy electrons appear to move inward to lower L shells faster than the higher energy electrons. However, the statistics of the data are consistent with the different behavior being due to spatial variations within the source mechanism as mentioned above.

March 2, 1965

The data for this storm, given in Figure 9, show a maximum intensity for all observed electrons at $L \simeq 4.5$. This agrees with the observed minimum shown in $t_{m/2}$ for low altitude mirroring electrons both at $\geq$280 keV and $\geq$1.2 MeV. The equatorial data are consistent with a minimum $t_{m/2}$ occurring over a relatively broad region at $L \gtrsim 4.5$ for the $\geq$300 keV electrons and beyond the observation region, $L > 5$, for the $\geq$1.0 MeV electrons.

The indication that the high altitude minimum $t_{m/2}$ may be displaced toward higher L shells from the low altitude minimum $t_{m/2}$ may be simply due to the geomagnetic field expansion during the storm main phase. That is, the low altitude and high altitude minimum $t_{m/2}$ actually occur in the same line of force but are labeled with different L values due to the field distortion. (Both 1963 38C and Explorer 26 use the same computer programs to calculate L value, given the position of the satellite.) This effect should be more apparent in $t_{m/2}$ than in the location of maximum intensity since $t_{m/2}$ generally occurs during the storm main phase whereas the maximum intensity, being affected by diffusion effects, may occur several days after the start of the storm.

March 22, 1965

The data for this storm are shown in Figure 10. Maximum intensities are observed in the vicinity of $L \simeq 5$ for all electrons.

The minimum $t_{m/2}$ shown by the lower energy electrons matches the position of maximum intensities for these particles. The low altitude $\geq$1.2 MeV data is not clear and the equatorial $\geq$1.0 MeV data show that if a minimum $t_{m/2}$ exists it is at or beyond L = 5.5. The differing characteristics of the $\geq$300 keV and $\geq$1.0 MeV $t_{m/2}$ plots may again be due to spatial variations in the source. For example, if no electrons greater than a few hundred kilovolts were directly produced in this storm, their appearance at the lower L shells would be due mainly to diffusion inward of an initially lower energy population. Moreover, the bulk of the observed higher energy electrons would be due to those lower energy electrons appearing at the outer edge of the main region of injection.

Figure 13 shows diffusion rates obtained from Figure 10 assuming that the apparent inward motion of the near-equatorial $\geq$1 MeV electrons is due solely to cross-L diffusion. The magnitude of the diffusion rates shown in Figure 13 are of the same order as those reported by Frank (1965) for the L $\sim$ 4.5 region. However, the $L^{-3}$ dependence shown in Figure 13 is in marked contrast to the $L^{-8}$ diffusion rate dependence observed by Frank (1965). This may be due to the fact that the diffusion rates reported here were obtained shortly after a magnetic disturbance and may thus be related to transient activity associated with the storm. Frank's (1965) observations were obtained over a several week period following an interval of enhanced magnetic activity and may thus represent more nearly quiescent magnetospheric conditions.

The situation with the low altitude $\geq$1.2 MeV electrons in Figure 10 is not clear since these regions are affected by diffusion down a flux tube as well as cross-L diffusion.

April 17, 1965

Figure 11 shows the electron data for this storm. Here the low altitude $\geq$280 keV electrons display a maximum intensity at L = 3.0 - 3.5 and the equatorial $\geq$300 keV electrons peak at L = 3.5. Both the $\geq$1.2 MeV electrons mirroring at 1100 km and the $\geq$1.0 MeV electrons mirroring near the equator show a major peak at L = 3.5.

All observed electrons display a well defined minimum $t_{m/2}$ at low L shells with the equatorial values being displaced toward higher L shells relative to the low altitude values.

This storm shows a well defined case of electrons initially appearing well within the trapping regions and subsequently diffusing in toward lower L shells and outward toward higher L shells (see also Figure 12). Note that the low altitude $\geq$280 keV data show a much steeper $t_{m/2}$ curve toward lower L values than toward higher L values, in qualitative agreement with diffusion theory under conservation of the first two adiabatic invariants. A similar observation was reported for the October 24, 1963 magnetic storm where the time interval, $T_D$, between peak magnetic activity and

attainment of peak $\geq$280 keV electron intensities was measured as a function of L (Williams and Smith, 1965). It was found that $T_D \sim 0.3$ days at L = 3, increased to $\sim$4.3 days at L = 2.5 and also continuously increased to $\sim$4 days as L increased to $\sim$9 earth radii.

Note also that all the data in Figure 11 show a definite change in character in the region of L = 4.5 - 5.5. The intensity plots either show a secondary maximum or a definite change of slope. The $t_{m/2}$ curves show either a secondary minimum or also a change of slope. We interpret this as evidence for a secondary appearance of electrons during this storm, occurring about 1.3 days after its start. Thus, Figure 11 shows a major arrival of energetic electrons occurring very shortly ($<$0.4 days) after the beginning of the storm in the region L $\simeq$ 3 - 3.5 followed by an apparent secondary appearance of energetic electrons about one day later at L $\sim$ 4.5 - 5.5.

The minimum $t_{m/2}$ values are not only displaced toward higher L shells at the equator but are also seen to have broader minima. This is in general agreement with the mapping of a flux tube from the equator to low altitudes during a period of enhanced field expansion. Figure 14 qualitatively illustrates this effect.

June 15, 1967

The data for this storm are shown in Figure 12. These data display broader maximum intensities and minimum $t_{m/2}$ curves than generally shown by the previous storms. In particular the $t_{m/2}$ plots indicate the arrival of energetic electrons at the equator and at low altitudes over a wide range of L values, but still within the trapping regions. The equatorial values are again displaced toward higher L shells for both the maximum intensity and minimum $t_{m/2}$. Also the L dependence of the slope of the $t_{m/2}$ plot is in qualitative agreement with cross-L diffusion theory as in the April 18 storm (see Figure 11).

All Storms

The energetic electron response to these main phase storms varies systematically with the size of the storm. To show this we have obtained from Figures 8-12, the L shell at which the minimum $t_{m/2}$ and maximum intensity occur. These L values (or their lower limits) are shown in Figure 15 for all energies and altitudes observed as a function of maximum Dst occurring during the storm. These maximum Dst values are listed for each storm in Table 2.

It is seen that the L value associated with the maximum intensity and earliest arrival of new energetic particles decreases as the size of the storm increases in agreement with previous low altitude results (Arens and Williams,

1967). In addition, the use of L as a parameter yields an apparent indication of the distortion present in the expanded field. The data associated with minimum $t_{m/2}$ in Figure 15 falls into two groups, the low altitude and the near-equatorial trapped electrons. Assuming that the energetic electrons first observed at both low and high altitudes are within the same flux tube, the $t_{m/2}$ data indicate that for a storm of $Dst^{max} \simeq -140\gamma$, an expansion of $\sim 0.5\ R_E$ occurs at an altitude of $\sim 3.2\ R_E$ while for a $Dst^{max}$ of $\simeq -30\gamma$ an expansion of $\simeq 0.2\ R_E$ occurs at $\sim 5.2\ R_E$. That is, a field line crossing the equator at $\sim 3.2\ R_E$ during quiescent conditions will cross the equator at $\sim 3.7\ R_E$ during a main phase storm when $Dst \simeq -140\gamma$.

The expansion shown in Figure 13 for the $140\gamma$ storm of April 17, 1965, agrees well with the more accurate values of $\Delta R \sim 1\ R_E$ at $R \sim 4\ R_E$ and $\Delta R \sim 0.5\ R_E$ at $R \sim 3R_E$ obtained by Davis (personal communication) utilizing field expansion data of Cahill (1966) obtained during this storm. The expansion noted at $\sim 5.2\ R_E$ for a $30\gamma$ storm is a lower limit since equatorial minimum $t_{m/2}$ were not observed within the region of observation.

The position of maximum intensity in Figure 15 does not display any readily discernable expansion effect. This is probably because the position of maximum intensity is strongly affected by diffusion down a flux tube and cross-L

diffusion. The minimum $t_{m/2}$ values are not significantly affected by these effects since they occur within 0.5 day of the beginning of the storm initial phase and, thus, before significant diffusion takes place.

Decay Times

Figures 2 and 3 show a variety of particle decreases including decay effects over an extended time period. Since the decay time measured by a threshold detector is affected in a complex way by energy loss mechanisms as well as particle transport processes, care has to be exerted in the interpretation of such decay times.

The lifetimes, $\tau$, for both the low altitude $\geq$280 keV electrons and the equatorial $\geq$300 keV electrons are shown in Figure 16 for two different time periods after the April 17, 1965 magnetic storm. The lifetime measured is the time for the electron intensities to reach $e^{-1}$ of their initial value.

The upper portion of Figure 16 shows a plot of $\tau$ vs L for the immediate post storm period, April 19 to 22.5, 1965. No points are shown for $L \geq 4.5$ since the intensities in these regions never decayed during the immediate post storm period. The bottom of Figure 16 shows $\tau$ vs L for the long term post storm period of April 22.5 to May 3, 1965. The error bars on the data points are not standard deviations but are upper and lower limits obtained by visually fitting the data points with a straight line on a logarithmic plot.

Not only do the low altitude and high altitude data display similar lifetimes for ~300 keV electrons, but their immediate post storm and long term post storm behavior agree. It is seen that immediately after the storm the decay times out to L = 3.5 are significantly shorter than the long term decay times. This effect is difficult to observe at L = 4 and no comparisons can be ma'e for L > 4.

This effect may simply be due to the fact that energy loss and particle transport mechanisms may be enhanced during the time when the magnetosphere is perturbed by the storm and as the storm subsides, the loss mechanisms and subsequent decay approach a more normal mode. The fact that Figure 16 shows this effect in the region around L = 3 may be due to this being the region of initial appearance of energetic electrons during the storm and thus probably the region of greatest magnetoelectric perturbations.

## DISCUSSION

### Losses

As pointed out earlier, Figures 2-5 show that generally the ~300 keV electrons on a given L shell rapidly ($\lesssim$1-2 days) come to equilibrium after a large geomagnetic storm, thereby causing the entire L shell to behave uniformly over extended periods of time. The differences in response on a particular L shell of the low altitude $\geq$280 keV electrons and the equatorial $\geq$300 electrons at the beginning of a storm may be due to (a) field expansions which invalidate a constant L label for an entire flux tube (Figure 15) and (b) the appearance of new particles having an anisotropic pitch angle distribution.

A good example of pitch angle effects during the appearance of new particles can be seen by examining the unidirectional electron data obtained by Explorer 26 at $L = 5\ R_E$ during the onset of the April 17 storm. Explorer 26 was at apogee during the onset of the storm and measured the first two hours of electron flux increases (Brown and Roberts, 1966). In addition to the omnidirectional measurements, the $\geq$450 keV electron flux was also sampled rapidly during one satellite rotation to give a measure of the unidirectional counting rate. This measured unidirectional data was reduced to absolute unidirectional flux as a function of the cosine of the electron pitch angle for each complete set of measurements taken during a satellite rotation.

Each set of unidirectional electron data was then fit by least squares (using two independent variables) to the function, flux = $A\left[1 - \frac{\mu_0^2}{\mu_{0C}^2}\right]^S$, (Roberts, 1965) where $\mu_0 = \cos \alpha_0$, $\alpha_0$ = equatorial pitch angle, and $\mu_{0C}$ is the loss cone. The variable A is for normalization purposes. Figure 17 contains a plot of the exponent S vs time during the April 17 storm. The behavior of S shows that the pitch angle distribution was initially peaked toward $\cos \alpha_0 = 0$ and changed to a rather uniform distribution over all pitch angles in certainly less than two hours and possibly less than one hour.

We thus conclude that equilibrium within a given flux tube is attained rapidly for >300 keV electrons ($\lesssim$0.1 day) and that the longer periods ($\sim$1-2 days) of nonuniform behavior on a given L shell (Figure 2) for $\gtrsim$300 keV electrons are due to field expansion during the storm (Figure 15).

The uniform behavior of the $\sim$300 keV electron population throughout a given flux tube causes the long term ($\gtrsim$0.5 day) diffusion and decay to appear pitch angle independent at these energies. It was seen above that the initial energization (injection) was pitch angle dependent but rapidly ($\lesssim$2 hours) reached an equilibrium distribution. The simplest conclusion to be drawn from these facts appears to be that the rapidity of the pitch angle diffusion mechanism causing electrons to diffuse down the line of force makes the slower processes (cross-L diffusion and decay) appear to be pitch angle independent.

The ~1 MeV electron population does not display the same general appearance of pitch angle independence for diffusion and decay as does the ~300 keV population. This can be seen from Figures 2-5 where the ~1 MeV electrons take significantly longer to attain equilibrium than do the ~300 keV electrons. In fact, Figure 4 shows a case where all 300 keV electrons are well into a decay mode along with the equatorial ~1 MeV electrons. However, the low altitude ~1.2 MeV electrons continue to increase.

The conclusion drawn here is that diffusion effects and decay times show a strong pitch angle dependence for ~1 MeV electrons because pitch angle diffusion mechanisms are not as effective in moving ~1 MeV electrons down a flux tube as they are for ~300 keV electrons.

Among possible pitch angle diffusion mechanisms, Roberts (1966, 1968) has discussed the scattering of relativistic electrons along a flux tube using cyclotron-resonance scattering by whistler-mode disturbances and bounce-resonance scattering by perturbations having electric or magnetic field components parallel to the local field. In particular, Roberts has considered these mechanisms operating with irregular, wide-band noise-like field fluctuations. Irregular whistler-mode disturbances with rms magnetic field fluctuations of order $>10^{-3}\gamma$ or bounce resonance scattering from irregular electric

field fluctuations of order $\geq 0.01$ V/km rms or magnetic intensity fluctuations of order $>10^{-5}$ rms of $B_{eq}$ yield pitch angle diffusion rates in rough agreement with observed outer zone electron lifetimes (Roberts, 1968). However the power spectral density functions which characterize the strength of the mechanism and determine the diffusion coefficients are not yet well known.

Both bounce-resonance and cyclotron-resonance scattering may be important in pitch angle diffusion since there may not be enough power available in the high frequency whistler region for the cyclotron-resonance interaction to effectively move particles with $\alpha_{eq} \sim \pi/2$ away from the equator.

If the above mechanisms are of major importance in pitch angle diffusion along a flux tube, then the fact that they apparently act more effectively for $\sim$300 keV electrons than $\sim$1 MeV electrons yields information concerning the respective power spectral density function.

We shall assume that these mechanisms are the dominant ones causing pitch angle diffusion for relativistic electrons. The less effective pitch angle diffusion for $\sim$1 MeV electrons may be due to (a) a reduced effectiveness of the bounce-resonance interaction in removing the electrons away from $\alpha_{eq} \sim \pi/2$ or (b) a reduced efficiency for the whistler mode

cyclotron-resonance interaction in lowering pitch angles ultimately into the loss cone. If case (a) prevailed and cyclotron-resonance scattering remained effective, then the low altitude electron intensities would closely follow equatorial intensities and there would be no build up of electron intensities at small pitch angles. This is not the case for the ~1 MeV particles and thus, case (b) seems applicable. It then follows that the power spectral density function for the wide band whistler mode noise interaction decreases in magnitude as those frequencies are approached which are responsible for the scattering of ~1 MeV electrons.

While whistler mode scattering is a strong function of cos $\alpha_{eq}$, the index of refraction, and the propagation direction of the wave relative to the local field direction, the following discussion may give certain limits concerning the power spectral density. The electrons not being scattered are ~1 MeV electrons mirroring at low altitude, cos $\alpha_{eq} \sim 1$. Using cos $\alpha_{eq} = 1$, an index of refraction $n \sim 10$, and assuming that the irregular whistler waves propagate nearly parallel to the field line, then the frequencies responsible for scattering an ~1 MeV electron in the cyclotron-resonance interaction are those in the region of 1 KHz at L = 3 and 200 Hz at L = 5.

The power spectral density function for the wide band whistler mode noise thus appears to have significantly less power at $\omega \approx 1$ KHz (corresponding to ~1 MeV electrons) than it has at $\omega \approx 2$ KHz (corresponding to ~300 keV electrons) at L = 3. The respective values at L = 5 are ~200 Hz (1 MeV electrons) and ~500 Hz (~300 keV electrons). While spatial dependencies in the power spectral density function will be important in determining equilibrium conditions over a wide range of altitudes, the present results indicate that the power spectral density function may decrease significantly in the region $\lesssim$1 KHz.

Figure 18 displays the measured decay times for the equatorially mirroring electrons at $\geq$300 keV, $\geq$450 keV and $\geq$1 MeV following the April 18, 1965 storm. The decays are measured during the long term post storm period, April 22.5 to May 3, 1965. It is seen that the $\gtrsim$1 MeV electrons display a longer lifetime throughout the $3 \leq L \leq 5$ region after this storm. In general, it was found that during the period under study, January 1 through June 29, 1965, whenever a persistent long term decay could be obtained for both electron energies, that the $\geq$1 MeV displayed the longer lifetime (e.g., Figure 4). The low altitude $\geq$1.2 MeV decay times are more difficult to obtain but where available show slightly longer lifetimes than the $\geq$280 keV electrons in the region $3 \leq L \leq 5$. Similar results have been observed for the period October 1 - 10, 1963 (Williams and Smith, 1965).

It thus appears that even during times well removed from major storms loss mechanisms in the $3 \lesssim L \lesssim 5$ region are less effective when operating on ~1 MeV electrons than on ~300 keV electrons. In light of the preceeding discussion, either the bounce-resonance interaction, or cross-L diffusion or both could be less effective at the higher energies.

It should be noted that the data of Figure 18 along with the $\geq$450 keV electron pitch angle data, Figure 17, indicate that the transitional energy region in the preceeding discussions is between 450 keV and 1 MeV. However since we only have low altitude data at $\geq$280 keV and $\geq$1.2 MeV, we shall continue to use $\gtrsim$300 keV and $\gtrsim$1.0 MeV as our reference energies.

Sources

It has been suggested that a source of energetic outer zone electrons is the cross-L diffusion, under conservation of the first two adiabatic invariants, of a low energy population initially located at the magnetospheric boundary

(Parker, 1960; Tverskoy, 1964). Such a process has been effectively employed in an attempt to arrive at an equilibrium outer zone proton distribution (Nakada and Mead, 1965). Observations indicating that such diffusion occurs for outer zone electrons have also been reported (Frank, 1965; Craven, 1966).

The observations reported hereing indicate that cross-L diffusion does play an important role in establishing an equilibrium outer zone electron distribution. However,, the initial appearance of energetic electrons well within the trapping regions and their subsequent diffusion toward lower and higher L shells shows that the above cross-L diffusion process need not be the major source of energetic electrons in the outer zone. The position at which energetic electrons are first seen within the trapping region and the variation of this position with the size of the storm (Figure 15) qualitatively can explain the dependence of outer zone electron intensity maxima on magnetic activity (McDiarmid and Burrows, 1967). In addition, the appearance of 1-3 MeV electrons at L values of ~8 earth radii may be explained without requiring electrons of a few hundred kilovolts at the boundary. These high L energetic electrons could be due to the outward diffusion of energetic electrons initially appearing at lower L shells.

The source of the energetic electrons initially appearing within the trapping region is unknown. The possible sources are (1) acceleration of the local plasma and (2) acceleration of a low energy population which is somehow transported in from other regions (e.g., the magnetotail).

Carpenter (1963, 1966), has interpreted ground based whistler data as indicating the existence of a sharp knee, the plasmapause, in the radial profile of electron density. The plasmapause, located at $\sim 4$ $R_E$ during periods of light magnetic activity, is thought to separate an inner region of $\sim$100 electrons/cc from an outer region of $\sim$1 electron/cc.

In discussing the distribution of electric fields in the magnetosphere, Block (1966) has reported that space charge effects will develop a central field free region within the magnetosphere and distribute the field toward the outer regions. He identifies the field free region with the above high density region within the plasmapause and considers that the possible low density region results from the electric fields in the outer magnetosphere sweeping away the local thermal plasma.

Carpenter (1966) has further observed an inward motion of the plasmapause during two periods of enhanced magnetic activity in July 1963. At this time the quiescent location of the whistler knee was at $\sim 5 - 5.5$ $R_E$. The

plasmapause was observed to move to the region 2.8 - 3.8 $R_E$ during the magnetic activity present on July 21, 22, and 30, 1963. The respective maximum Dst values were -23$\gamma$, -30$\gamma$, and -20$\gamma$ (Suguira and Hendricks, 1966). The trapped electron data in Figure 15 indicate that for $Dst^{max}$ of -20$\gamma$ to -30$\gamma$, energetic electrons are first seen at $L > 5\ R_E$. The appearance of energetic electrons during small magnetic disturbances is thus seen to occur well above the region to which the whistler knee is observed to move. That is, the energetic electron population is observed in the low density region as discussed by Carpenter (1963) or, equivalently, in the field region as described by Block (1966).

Bauer and Krishnamurthy (1968a) have suggested an alternative explanation for the existence of a whistler cutoff, i.e., plasmapause, during magnetic storms. They argue that the absence of whistler propagation above a certain altitude (L shell) may be due to the absorption of these waves via Landau damping by intense energetic electron fluxes appearing within the ring current region during a storm.

The present energetic electron observations are consistent with this possibility in that for the -20$\gamma$ to -30$\gamma$ storms reported (Carpenter, 1966), the whistler knee was observed to move to lower altitudes from an ambient value which is coincident, within the allowable errors, with the

initial appearance of energetic electrons. The appearance of energetic electrons may thus damp the waves and thus cause the observed lowering of the knee.

If during quiet times, the ambient plasma density on the high altitude side of the plasmapause is $\sim 1$ cm$^{-3}$ (Carpenter, 1963), then it is not possible to obtain from the local plasma the low energy particle intensities thought to be responsible for the ring current (Hoffman and Bracken, 1965; Frank, 1967). It is possible however with these low plasma densities to support the energetic ($\gtrsim$ 280 keV) electron population found in these regions during storms. Therefore, the primary acceleration mechanism responsible for the freshly observed energetic electrons during a main phase storm, which seems to reside within the trapping regions but above the whistler knee, can use both local plasma and transported plasma as a major source of particles.

The response of the topside ionosphere during the April 17, 1965 magnetic storm has been reported by Bauer and Krishnamurthy (1968b). Both enhancements and depletions of topside ionization were observed and were found to depend on the phase of the storm. In particular, a large depletion in the maximum electron density Nm F2 was associated with the main phase expansion of the field at the time of the symmetric phase of the ring current. The peak depletion was observed

to occur at L = 3, in excellent agreement with the initial appearance of energetic electrons at 1100 km and the location of their maximum intensity (Figure 11). Bauer and Krishnamurthy (1968b) suggest that this depletion represents an upward flux of plasma caused by reduced plasma densities at high altitudes due to either the main phase field expansion or to the acceleration of the local thermal plasma. The present results indicate that a major acceleration mechanism can operate within the stable trapping regions and initially at high altitudes.

If the local plasma were energized, a local low energy depletion could result due to the energization and to field expansion caused by the energized particles. This in turn could cause an upward flow of ionospheric plasma to these regions and yield the Nm F2 depletions observed in the ionosphere (Bauer and Krishnamurthy, 1968b). The spatial correlation of the equatorial and low altitude energetic trapped electron results and the simultaneous Nm F2 depletion results during the April 17, 1965 magnetic storm are consistant with such a process. The equivalent low altitude and equatorial regions may be obtained roughly from Figures 11, 14 and 15.

Thus the creation of intense energetic particle populations within the magnetosphere may stem from a variety of sources (e.g., local plasma, a low energy population from the magnetotail, ionospheric effects).

Many of these effects (decay, cross-L diffusion, pitch angle diffusion, acceleration, etc.) may well be storm dependent. The power spectral density function, for example, may vary from storm to storm and may also have a different shape during quiet times. This would have the effect of varying the energy at which pitch angle diffusion would become effective as a function of some as yet unknown storm parameter. Simultaneous particle-wave-field observations over many storms are required in order to identify the more significant sources and losses throughout the outer zone. The difficulty of these identifications is emphasized by the iterative nature of these mechanisms; i.e., sufficient particle intensities and anisotropies may trigger instabilities which produce the diffusion leading to the loss of the initial particles (Kennel and Petchek, 1966).

Similar particle-field-wave-plasma observations for a variety of storms will be invaluable in furthering understanding of the relation between magnetospheric plasma and energetic particles associated with the stable trapping region.

SUMMARY

Simultaneous data have been presented for trapped electrons at energies $\gtrsim$280 keV and $\gtrsim$1 MeV as observed throughout much of the outer zone at 1100 km by the satellite 1963 38C and in the near equatorial regions by the Explorer 26 satellite. These observations were obtained during the time period January 1 through June 29, 1965, for the L values 3.0, 3.5, 4.0, 4.5, 5.0 and 5.5 earth radii. The behavior of the trapped electron intensities were studied and discussed during five well defined magnetic storms which were accompanied by electron intensity increases throughout much of the region of observation. The following results and conclusions were obtained:

(1) The $\gtrsim$300 keV trapped electrons on a given L shell (Figure 2) rapidly ($\lesssim$1-2 days) come to equilibrium after a large magnetic disturbance, thereby causing the entire L shell to behave uniformly over extended periods of time.

(2) Pitch angle data for near equatorially mirroring $\gtrsim$450 keV electrons during the April 18, 1965 storm indicate that these electrons rapidly ($\lesssim$0.1 day) come to equilibrium within a given flux tube.

(3) It is thus concluded that the $\gtrsim$300 keV electrons also come to equilibrium within a given flux tube within ~0.1 days and that the longer (~1-2 day) noruniform behavior on a given L shell (Figure 2) is due to field expansion during the storm (see number 10 below).

(4) It is further concluded that the longer term (many day) cross-L diffusion and decay processes acting on $\gtrsim$300 keV electrons appear pitch angle independent due to the rapidity of the pitch angle diffusion mechanisms which strongly couple >300 keV electron intensities all along the line of force.

(5) Such an apparent pitch angle independence for the long term cross-L diffusion and decay processes is not observed for the $\gtrsim$1 MeV electrons.

(6) It is thus concluded that pitch angle diffusion mechanisms are not as effective in lowering the mirror points of $\gtrsim$1 MeV electrons as they are for $\gtrsim$300 keV electrons. It is this energy dependence of the pitch angle scattering mechanisms that allows the observation of a strong pitch angle dependence for cross-L diffusion and decay effects at $\gtrsim$1 MeV.

(7) Using the cyclotron and bounce-resonance interactions with wide band irregular field fluctuations, as described by Roberts (1968), as major loss mechanisms, it is found that the power spectral density function characterizing the cyclotron-resonance interaction may decrease significantly in magnitude as the frequency is lowered from $\omega \sim 1000 - 2000$ Hz to $\omega \sim 200 - 1000$ Hz.

(8) Longer lifetimes are observed for $\gtrsim$1 MeV electrons than for $\gtrsim$300 keV electrons, indicating that either cross-L diffusion or the bounce-resonance interaction may be less effective at higher energies.

(9) Shorter lifetimes for both low and high altitude trapped $\gtrsim$300 keV electrons were observed immediately ($\lesssim$5 days) after the April 17 storm than during the long term (5 to 16 days) post storm period (Figure 16). This effect was seen in the region $L \sim 3\ R_E$ where the storm produced its largest energetic particle effects. The shorter lifetime in the immediate post storm period may be due to an enhancement of loss processes during disturbed periods.

(10) Measuring the time required for the electron intensities to reach one-half their maximum value, $t_{m/2}$, after the start of a storm has led to the result that energetic ($\gtrsim$300 keV, $\gtrsim$1 MeV) electrons associated

with a main phase magnetic disturbance may initially appear well within the trapping regions and subsequently diffuse both in towards lower L values and out towards higher L values. A case of a possible double appearance of energetic electrons was found in the April 17, 1965 storm.

(11) It was also observed that the minimum $t_{m/2}$ and maximum intensity at both low and high altitude occurred at lower L values as the maximum Dst of the storm increased. This is in agreement with previous low altitude results (Arens and Williams, 1967). It was further observed that the equatorial and low altitude minimum $t_{m/2}$ values fell on separate curves (Figure 15) on a L vs $Dst^{max}$ plot. This is interpreted as a measure of field expansion during the storm and yields $\Delta R \gtrsim 0.2\ R_E$ at $R \sim 5\ R_E$ for $Dst^{max} = -30\gamma$ and $\Delta R \sim 0.5\ R_E$ at $R \sim 3.2\ R_E$ for $Dst^{max} = -140\gamma$. The latter value agrees well with the $\Delta R \sim 0.5\ R_E$ at $R = 3.5\ R_E$ obtained by Davis (personal communication) during the same April 17, 1965, storm included in this study.

(12) The appearance of energetic electrons within the trapping regions and its variation with $Dst^{max}$ coupled with the subsequent transport of these

electrons can qualitatively explain the dependence of outer zone electron intensity maxima on magnetic acitivity (McDiarmid and Burrows, 1967). These observations can also explain the appearance of several MeV electrons at L values of ~8 $R_E$ without requiring a several hundred kilovolt population at magnetospheric boundary.

(13) Preliminary evidence indicates that the energetic electrons initially appear on the high altitude side of the whistler knee, i.e., on the low density side of the plasmapause as discussed by Carpenter (1963). The motion of the whistler knee to lower altitudes during small magnetic storms (Carpenter, 1963) coupled with the region of appearance of energetic ($\gtrsim$300 keV) electrons during similar size storms lends support to the suggestion of Bauer and Krishnamurthy (1968a) that, during storms, the whistler cutoff and the apparent motion of the whistler knee is due to the appearance of energetic electrons associated with the storm ring current which absorbs the waves via Laundau damping.

(14) The depletion in the topside ionosphere maximum electron density, Nm F2, was observed to peak at L = 3 during the April 17, 1965 magnetic storm (Bauer and Krishnamurthy, 1968b). This region of

peak Nm F2 depletion agrees very well with the region of minimum $t_{m/2}$ and maximum intensity observed for the low altitude energetic electrons during this same storm (Figure 11). The energetic electrons during the April 17, 1965, magnetic storm appeared initially well within the trapping regions (L = 3 at 1100 km) and were thus produced by an acceleration mechanism acting in these regions on either the local low energy population or on a low energy population transported in from elsewhere.

ACKNOWLEDGMENTS

It is a pleasure to acknowledge the stimulating and helpful discussions held with Drs. C. S. Roberts and S. J. Bauer.

We wish to express our appreciation to Drs. S. Hendricks and M. Sugiura for making the hourly Dst averages for 1965 available to us prior to publication and to Dr. D. H. Fairfield for making the AE indices available.

The help of Miss C. G. Maclennan in analyzing the Explorer 26 pitch angle data is greatly appreciated.

Figure 1. Projection onto ecliptic plane of Explorer 26 and 1963 38C orbits showing local times sampled by these satellites during the six month period of January-June 1965.

Figure 2. Simultaneous electron data from the polar orbiting satellite 1963 38C (E > 280 keV) and the near equatorial satellite Explorer 26 (E > 300 keV) for the period January 1, 1965, through June 29, 1965. The electron data at L = 3.0, 3.5, 4.0, 4.5, 5.0, and 5.5 are shown in terms of counts for each of the experiments counting intervals. See Table 1 for the conversion factors to convert the data to fluxes. Below the electron data are plotted the hourly average Dst and the three hour average Kp index for the six month period.

Figure 3. Simultaneous electron data from the polar orbiting satellite 1963 38C (E > 1.2 MeV) and the near equatorial satellite Explorer 26 (E > 1.0 MeV) for the period January 1, 1965, through June 29, 1965. The electron data at L = 3.0, 3.5, 4.0, 4.5, 5.0, and 5.5 are shown in terms of counts for each of the experiments counting intervals. See Table 1 for the conversion factors to convert the data to fluxes. Below the electron data are plotted the hourly average Dst and the three hour average Kp index for the six month period.

Figure 4. Simultaneous electron data from the polar orbiting satellite 1963 38C (E > 280 keV and E > 1.2 MeV) and the near equatorial satellite Explorer 26 (E > 300 and E > 1.0 MeV) for March 1 through March 12, 1965. Electron data at L = 4.0, 4.5, and 5.0 is shown during the period of the March 3 geomagnetic storm. Below the electron data are plotted the AE index, Dst, and the Kp index.

Figure 5. Simultaneous electron data from the polar orbiting satellite 1963 38C (E > 280 keV and E > 1.2 MeV) and the near equatorial satellite Explorer 26 (E > 300 keV and E > 1.0 MeV) for June 13 through June 25, 1965. Electron data at L = 3.5, 4.0, 4.5, 5.0, and 5.5 are shown during the period of the June 15 geomagnetic storm. Below the electron data are plotted the AE index, Dst, and the Kp index.

Figure 6. Sequence of low altitude trapped electron outer zone profiles obtained by satellite 1963 38C during February 6, 1965, magnetic storm. Numbered arrows in plot of Dst and AE values indicate time sequence of respective numbered passes. Note initial high latitude appearance of electrons associated with substorm during main [illegible]d compression, their

subsequent loss to these low altitude regions, and the later arrival of the bulk of energetic electrons associated with the storm main phase.

Figure 7. Simultaneous electron data from 1963 38C (E > 280 keV) and Explorer 26 (E > 300 keV) during the February 6, 1965, geomagnetic storm. Below the electron data are the AE and Kp indices and the equatorial Dst. The equatorial electron data shows the first particle increases at L = 5, apparently correlated with the AE spike at the time of the sudden commencement. The low altitude electron data also indicate an increase at this time. However a decrease occurs after this substorm but before the storm main phase and major electron increase (see also Figure 6). Equatorial data are not available during this time interval.

Figure 8. February 6, 1965, Geomagnetic Storm: The maximum storm electron intensities and the time required for the intensities to reach half their peak values ($t_{m/2}$) plotted vs L for the high and low energy electrons observed on 1963 38C and Explorer 26. Explorer 26 $\geq$300 keV and $\geq$1.0 MeV data has been multiplied by 0.1 and 1963 38C $\geq$1.2 MeV data has been multiplied by 5. Using these factors, fluxes may be obtained from the conversion constants in Table 1.

Figure 9. March 2, 1965, Geomagnetic Storm: The maximum storm electron intensities and the time required for the intensities to reach half their peak values ($t_{m/2}$) plotted vs L for the high and low energy electrons observed on 1963 38C and Explorer 26. Explorer 26 $\geq$300 keV data has been multiplied by 0.1 and 1963 38C $\geq$1.2 MeV data has been multiplied by 10. Using these factors, fluxes may be obtained from the conversion constants in Table 1.

Figure 10. March 22, 1965, Geomagnetic Storm: The maximum storm electron intensities and the time required for the intensities to reach half their peak values ($t_{m/2}$) plotted vs L for the high and low energy electrons observed on 1963 38C and Explorer 26. Explorer 26 $\geq$300 keV data has been multiplied by 0.1 and 1963 38C $\geq$1.2 MeV data has been multiplied by 10. Using these factors, fluxes may be obtained from the conversion constants in Table 1.

Figure 11. April 17, 1965, Geomagnetic Storm: The maximum storm electron intensities and the time required for the intensities to reach half their peak values ($t_{m/2}$) plotted vs L for the high and low energy electrons observed on 1963 38C and

and Explorer 26. Explorer 26 $\geq$300 keV data has been multiplied by 0.1 and 1963 38C $\geq$1.2 MeV data has been multiplied by 10. Using these factors, fluxes may be obtained from the conversion constants in Table 1. A possible second appearance of electrons was observed in the region L = 4.5 - 5.5.

Figure 12. June 15, 1965, Geomagnetic Storm: The maximum storm electron intensities and the time required for the intensities to reach half their peak values ($t_{m/2}$) plotted vs L for the high and low energy electrons observed on 1963 38C and Explorer 26. Explorer 26 $\geq$300 keV and $\geq$1.0 MeV data has been multiplied by 0.1. Using these factors, fluxes may be obtained from the conversion constants in Table 1. A very broad region (L = 3.5 - 5.0) of initial electron appearance was observed.

Figure 13. Rate of apparent inward motion for the equatorial E > 1.0 MeV electrons plotted vs L from the March 22, 1965, geomagnetic storm (Figure 10). These data show the clearest example of possible inward electron diffusion for the storms examined. Plots of $dL/dt = L^n$ for several values of n are shown along with the data.

Figure 14. Diagram, not to scale, qualitatively showing the projection of a wide source region in equatorial regions to a narrow latitude interval at low altitudes. Projection during a main phase field expansion shown as cross-hatched section. Dipole projection shown as shaded section for comparison.

Figure 15. a. The L value of maximum electron intensity plotted vs the peak Dst value for the five geomagnetic storms examined in Figures 8-12. Both energies at both low and high altitudes are included.

b. The L value of the earliest $t_{m/2}$ plotted vs the peak Dst value for the same five geomagnetic storms. A separation, attributable to a measure of the magnetospheric expansion, is observed between the high and low altitude electron data.

Figure 16. Lifetimes (time to $e^{-1}$ of initial value) for energetic electrons plotted vs L for two periods following the April 17, 1965, geomagnetic storm.

a. Lifetimes for the immediate post-storm period, April 19 - April 22.5, 1965. Data beyond L = 4.0 was not available because outward electron diffusion was still operative during portions of this time period at the higher L values and no decay was observed.

b. Lifetimes for the post storm period April 22.5 - May 3, 1965. The decay rates at the low L values have increased by a factor of about 2 over the rates in (a) at L = 2.6 - 3.5. At all L values, for both periods of time, the decay rates observed for these energetic electrons at high and low latitude are nearly identical.

Figure 17. Plot of the value of the exponent s in the fit to the pitch angle electron data ($E > 0.45$ MeV) vs time during the onset of the April 18, 1965, geomagnetic storm near L = 5 $R_E$. The exponent s very rapidly tends toward the quiet time value after the L = 5 storm onset at about 0620. This indicates that an initial electron population, peaked in pitch angle distribution at the equator, rapidly changes to a rather uniform electron flux population over all pitch angles.

Figure 18. Near-equatorial electron lifetimes for $E > 300$ keV, >450 keV, and >1.0 MeV plotted vs L for the period April 22.5 - May 3, 1965 (Figure 16b). The $E > 1.0$ MeV electrons display a longer lifetime in the region L = 3.0 - 5.0 during this time period.

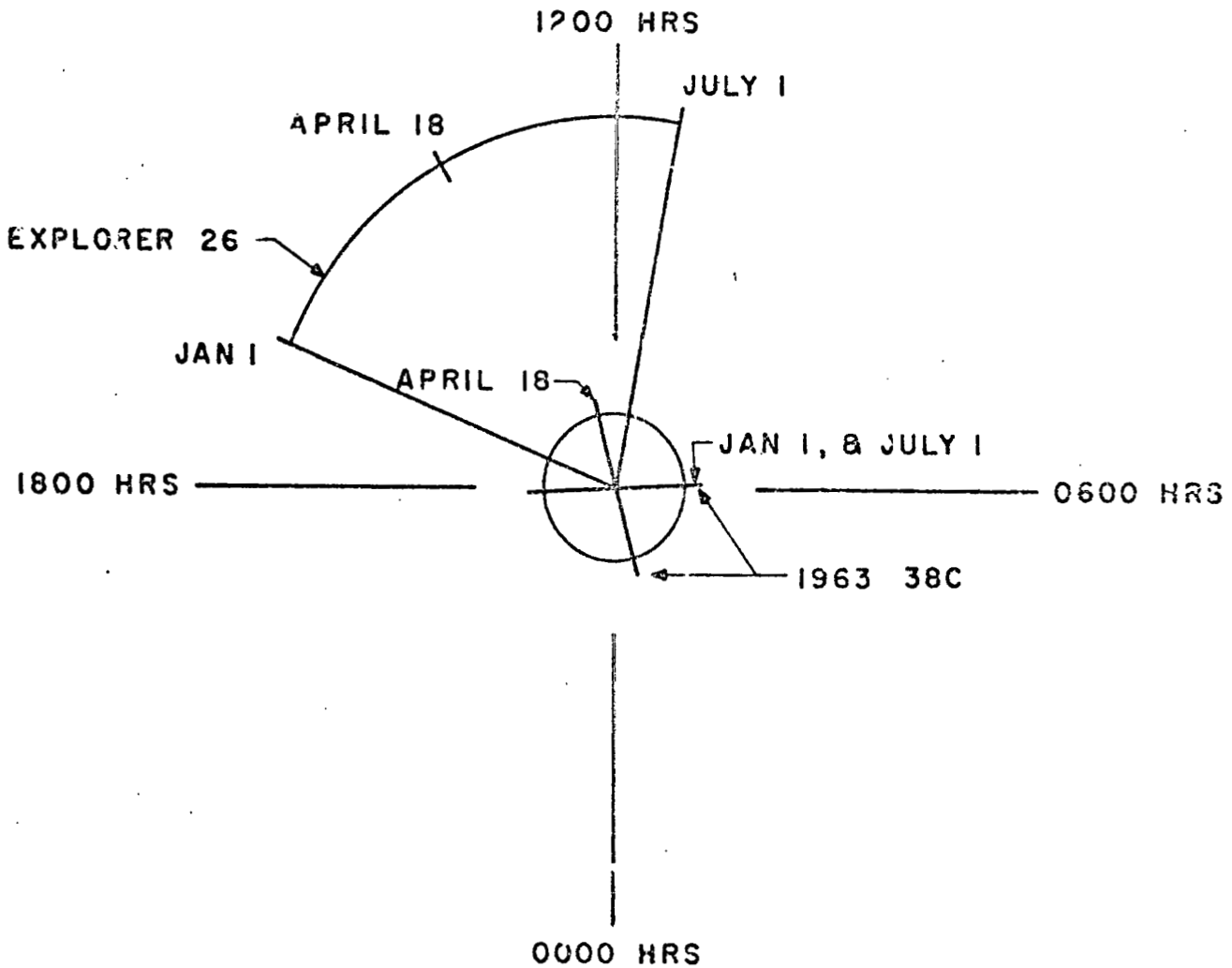


LOCAL TIMES SAMPLED
JAN-JULY 1965

Figure 1

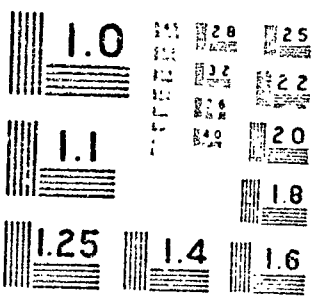

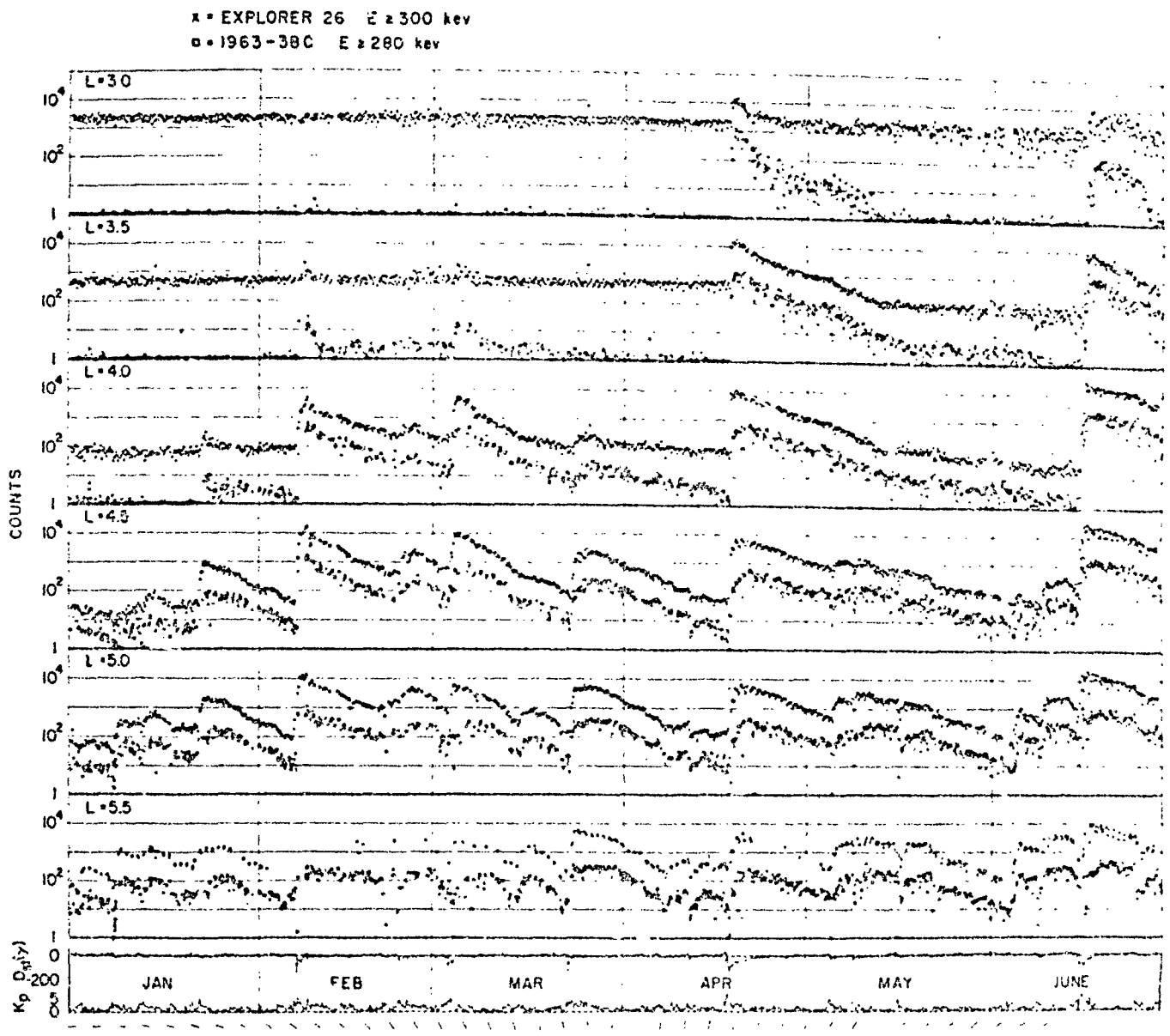
x = EXPLORER 26 E ≥ 300 kev
o = 1963-38C E ≥ 280 kev
L=3.0
L=3.5
L=4.0
L=4.5
L=5.0
L=5.5
COUNTS
JAN
FEB
MAR
APR
MAY
JUNE

Figure 2

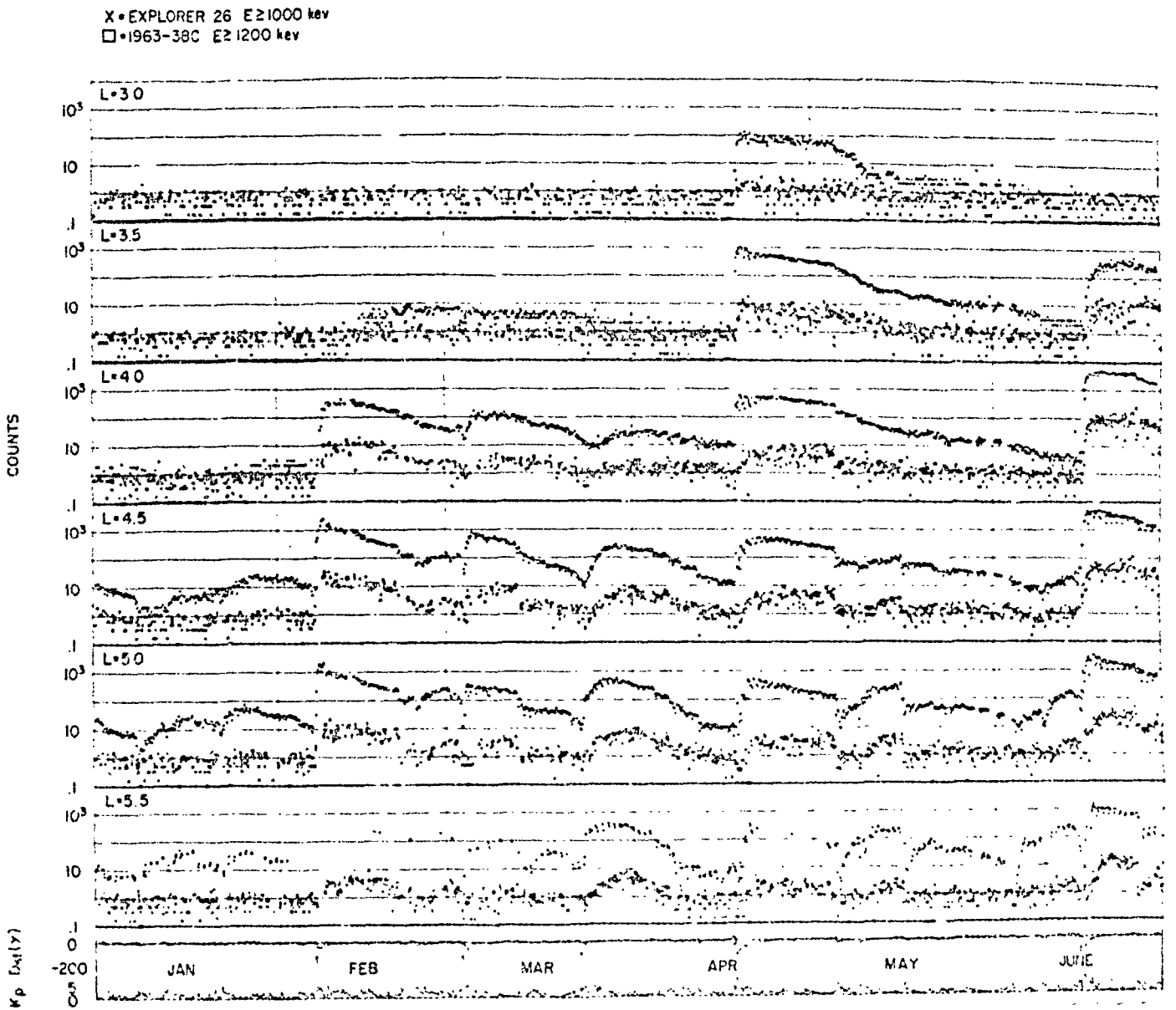
X • EXPLORER 26 E ≥ 1000 kev
□ • 1963-38C E ≥ 1200 kev
L • 3.0
L • 3.5
L • 4.0
L • 4.5
L • 5.0
L • 5.5
COUNTS
JAN
FEB
MAR
APR
MAY
JUNE

Figure 3

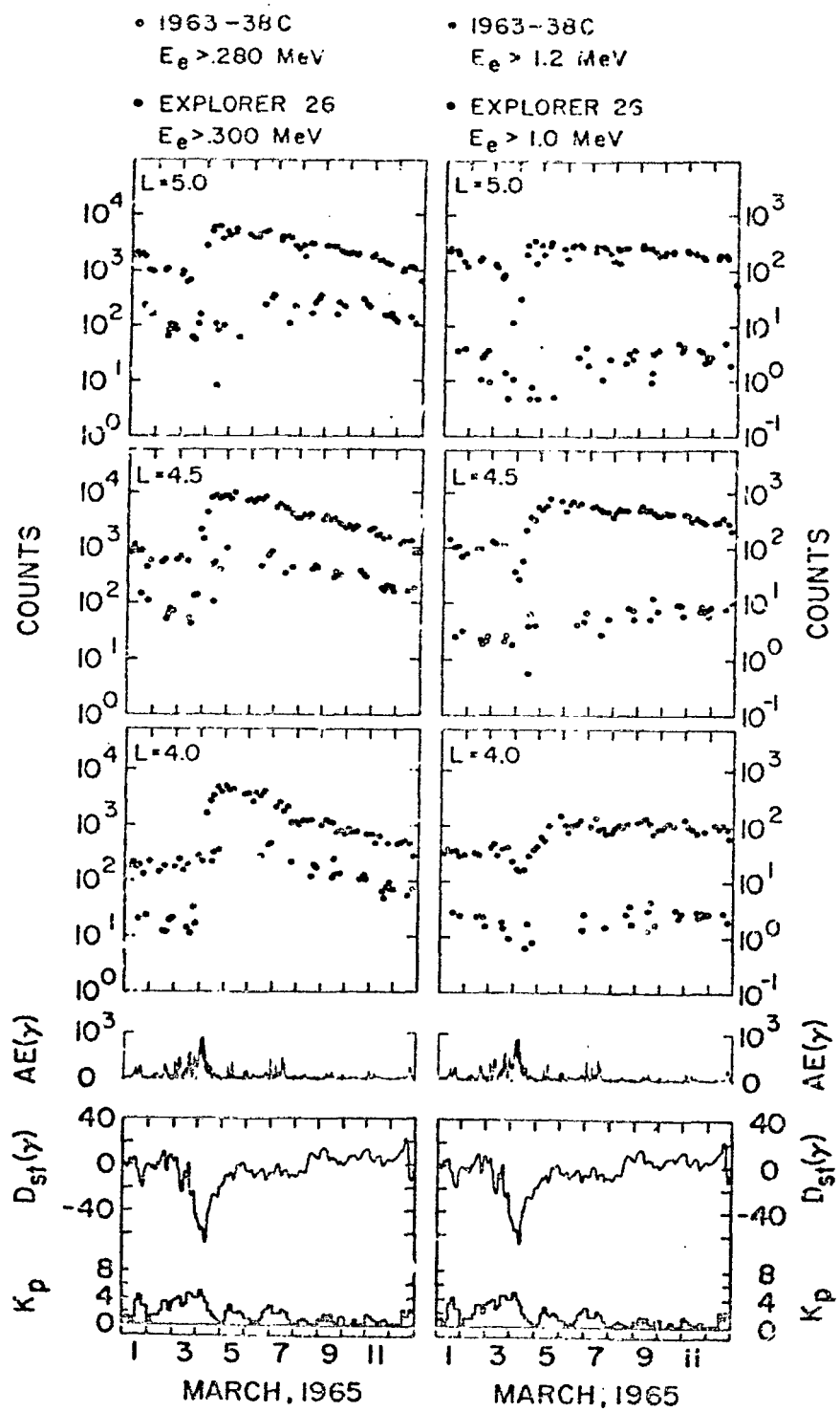
• 1963-38C
$E_e$ > .280 MeV
• EXPLORER 26
$E_e$ > .300 MeV
• 1963-38C
$E_e$ > 1.2 MeV
• EXPLORER 26
$E_e$ > 1.0 MeV
L=5.0
L=4.5
L=4.0
COUNTS
AE(γ)
$D_{st}$(γ)
$K_p$
1 3 5 7 9 11
MARCH, 1965

Figure 4

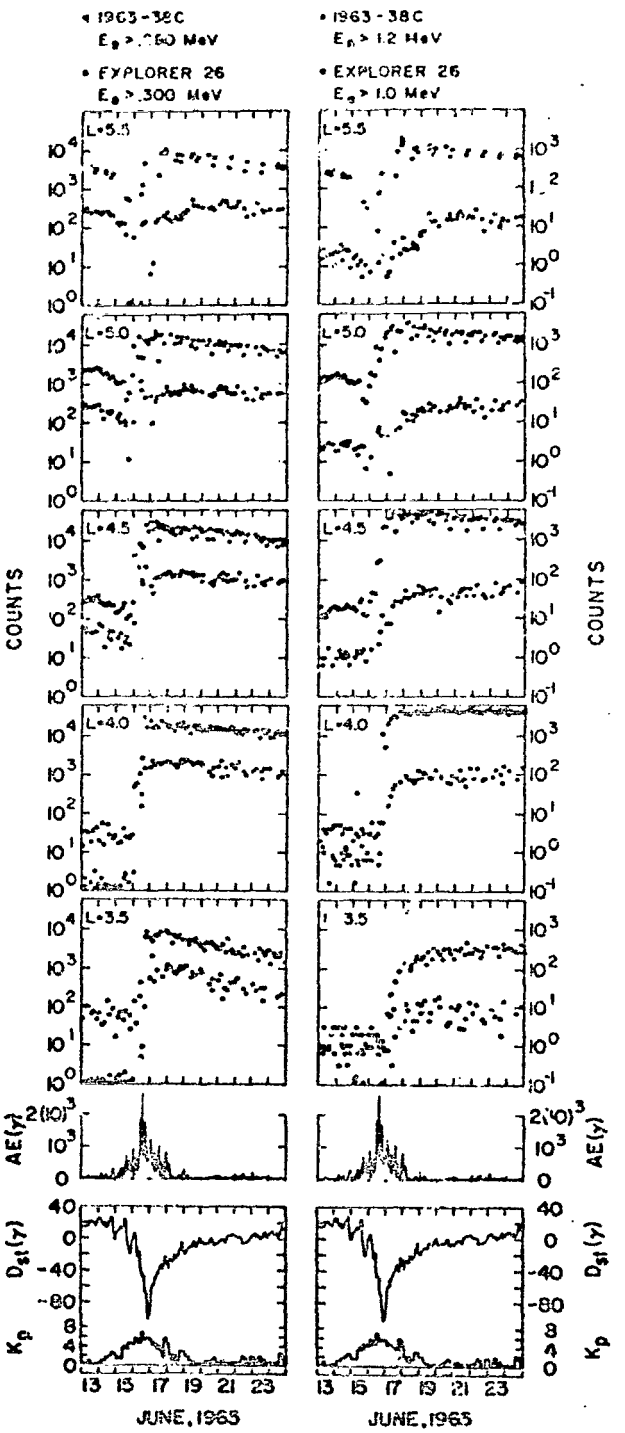
• 1963-38C
$E_e$ > .150 MeV
• EXPLORER 26
$E_e$ > .300 MeV
• 1963-38C
$E_e$ > 1.2 MeV
• EXPLORER 26
$E_e$ > 1.0 MeV
L=5.5
L=5.0
L=4.5
L=4.0
L=3.5
COUNTS
AE(γ)
$D_{st}(\gamma)$
$K_p$
13 15 17 19 21 23
JUNE, 1965

Figure 5

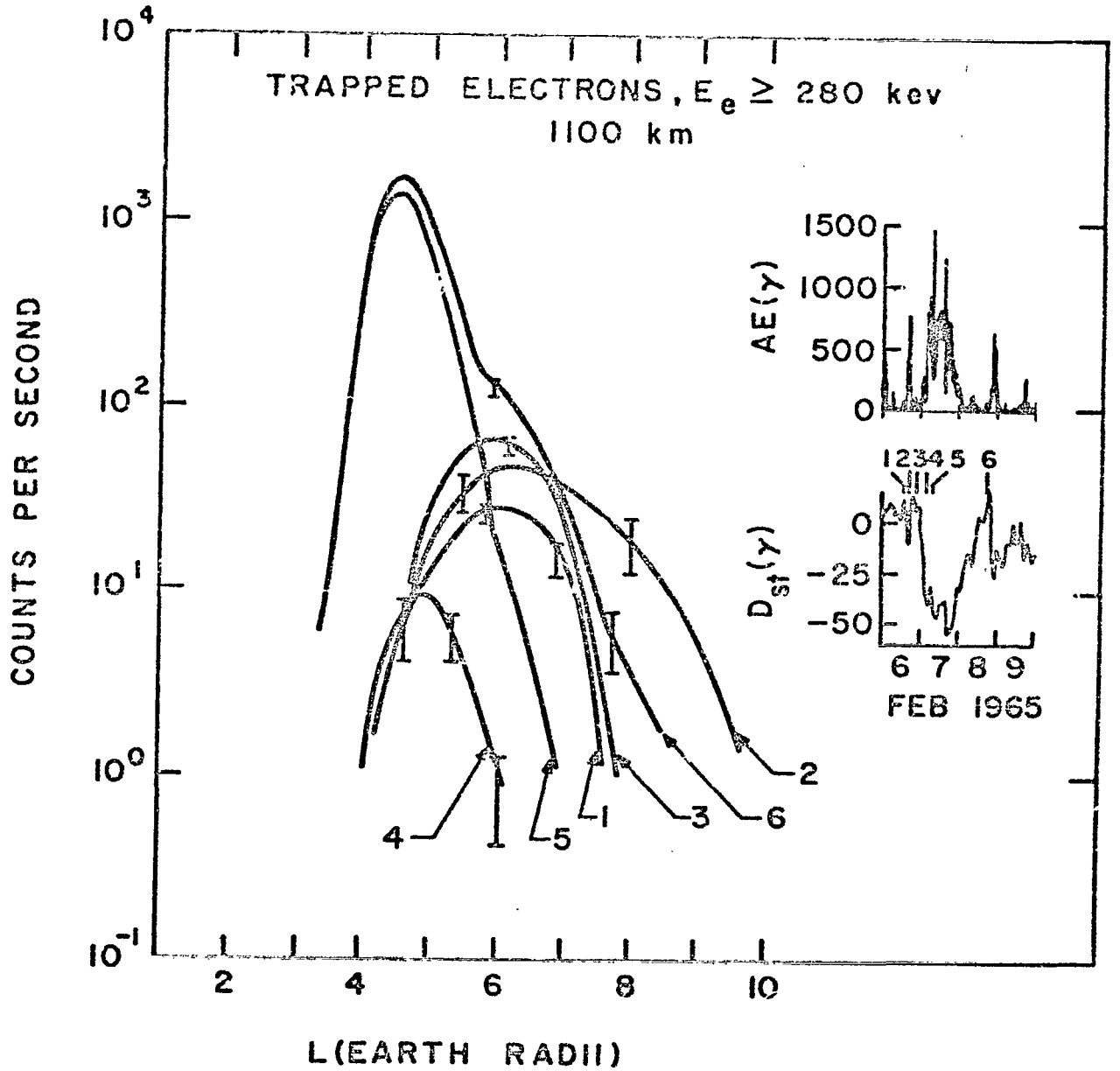
TRAPPED ELECTRONS, $E_e \geq 280$ kev
1100 km
COUNTS PER SECOND
$10^4$
$10^3$
$10^2$
$10^1$
$10^0$
$10^{-1}$
2
4
6
8
10
L(EARTH RADII)
1
2
3
4
5
6
AE(γ)
1500
1000
500
0
$D_{st}$(γ)
0
-25
-50
1 2 3 4 5 6
6 7 8 9
FEB 1965

Figure 6

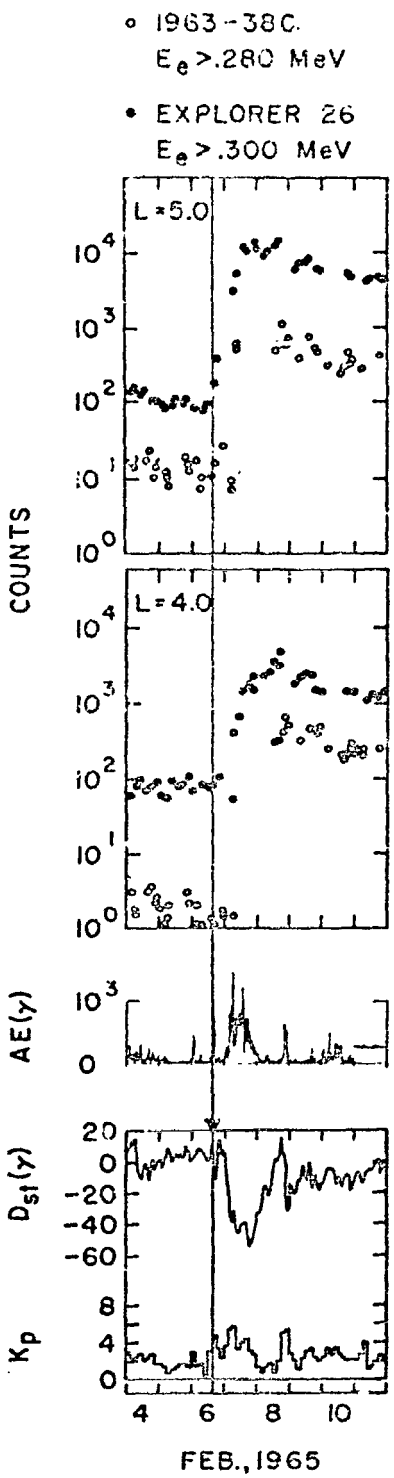
○ 1963-38C.
$E_e$ >.280 MeV
• EXPLORER 26
$E_e$ >.300 MeV
L=5.0
L=4.0
COUNTS
AE(γ)
$D_{st}$(γ)
$K_p$
FEB., 1965

Figure 7

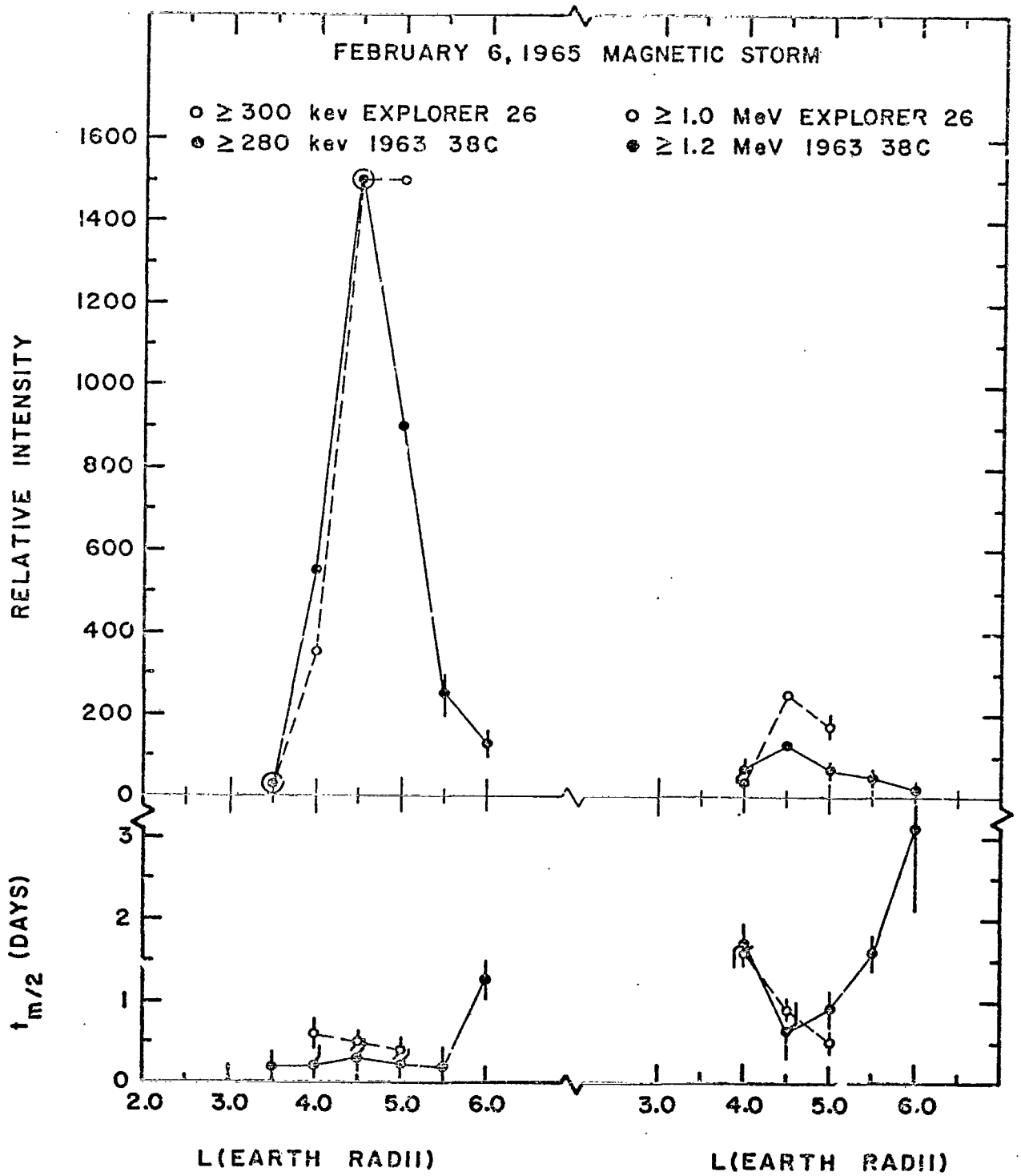
FEBRUARY 6, 1965 MAGNETIC STORM
o ≥ 300 kev EXPLORER 26
• ≥ 280 kev 1963 38C
o ≥ 1.0 MeV EXPLORER 26
• ≥ 1.2 MeV 1963 38C
RELATIVE INTENSITY
1600
1400
1200
1000
800
600
400
200
0
$t_{m/2}$ (DAYS)
3
2
1
0
2.0
3.0
4.0
5.0
6.0
3.0
4.0
5.0
6.0
L(EARTH RADII)
L(EARTH RADII)

Figure 8

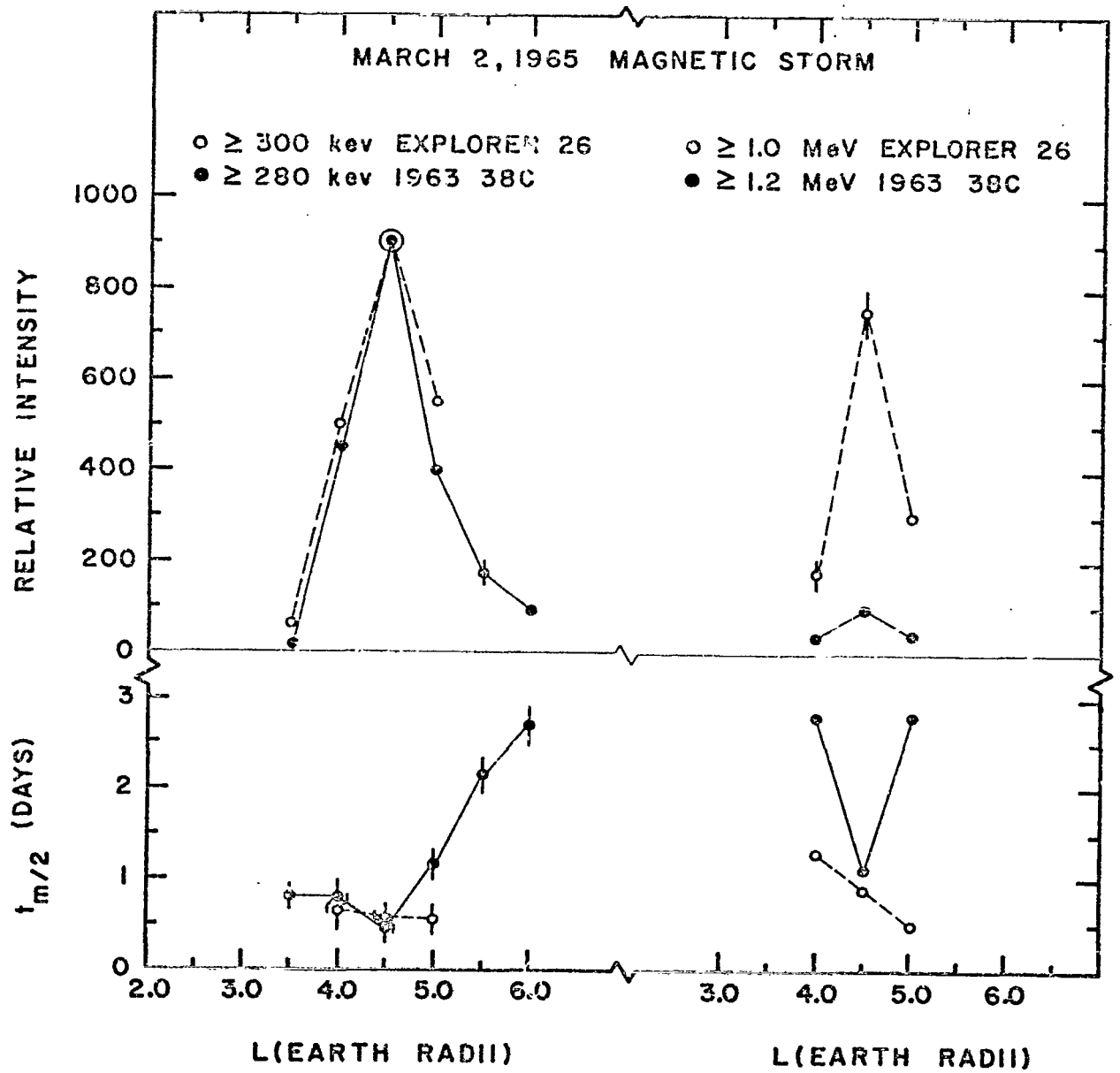
MARCH 2, 1965 MAGNETIC STORM
o ≥ 300 kev EXPLORER 26
● ≥ 280 kev 1963 38C
o ≥ 1.0 MeV EXPLORER 26
● ≥ 1.2 MeV 1963 38C
RELATIVE INTENSITY
1000
800
600
400
200
0
$t_{m/2}$ (DAYS)
3
2
1
0
2.0
3.0
4.0
5.0
6.0
3.0
4.0
5.0
6.0
L(EARTH RADII)
L(EARTH RADII)

Figure 9

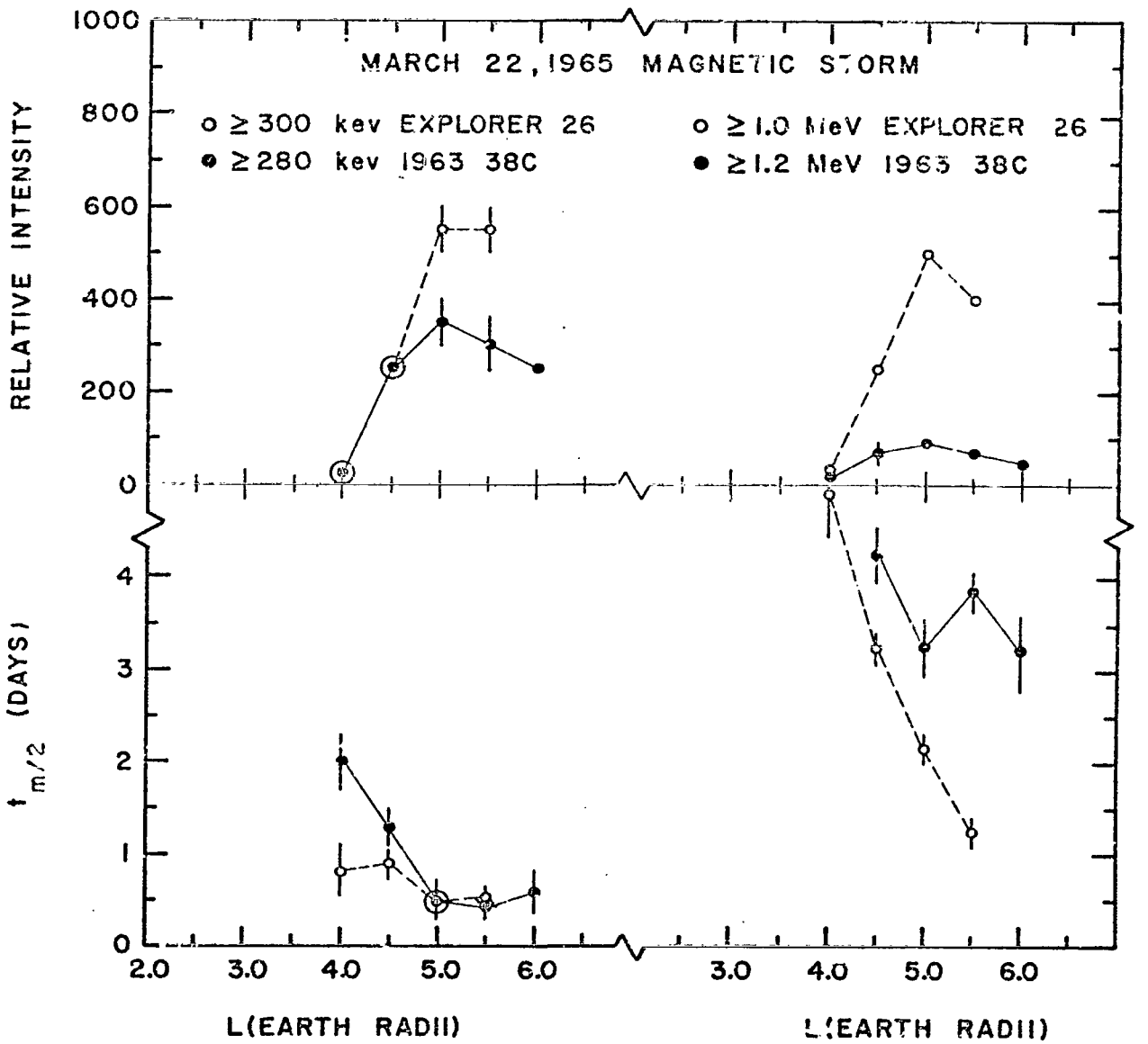
MARCH 22, 1965 MAGNETIC STORM
o ≥ 300 kev EXPLORER 26
• ≥ 280 kev 1963 38C
o ≥ 1.0 MeV EXPLORER 26
• ≥ 1.2 MeV 1963 38C
RELATIVE INTENSITY
1000
800
600
400
200
0
$t_{m/2}$ (DAYS)
4
3
2
1
0
2.0
3.0
4.0
5.0
6.0
L(EARTH RADII)
3.0
4.0
5.0
6.0
L(EARTH RADII)

Figure 10

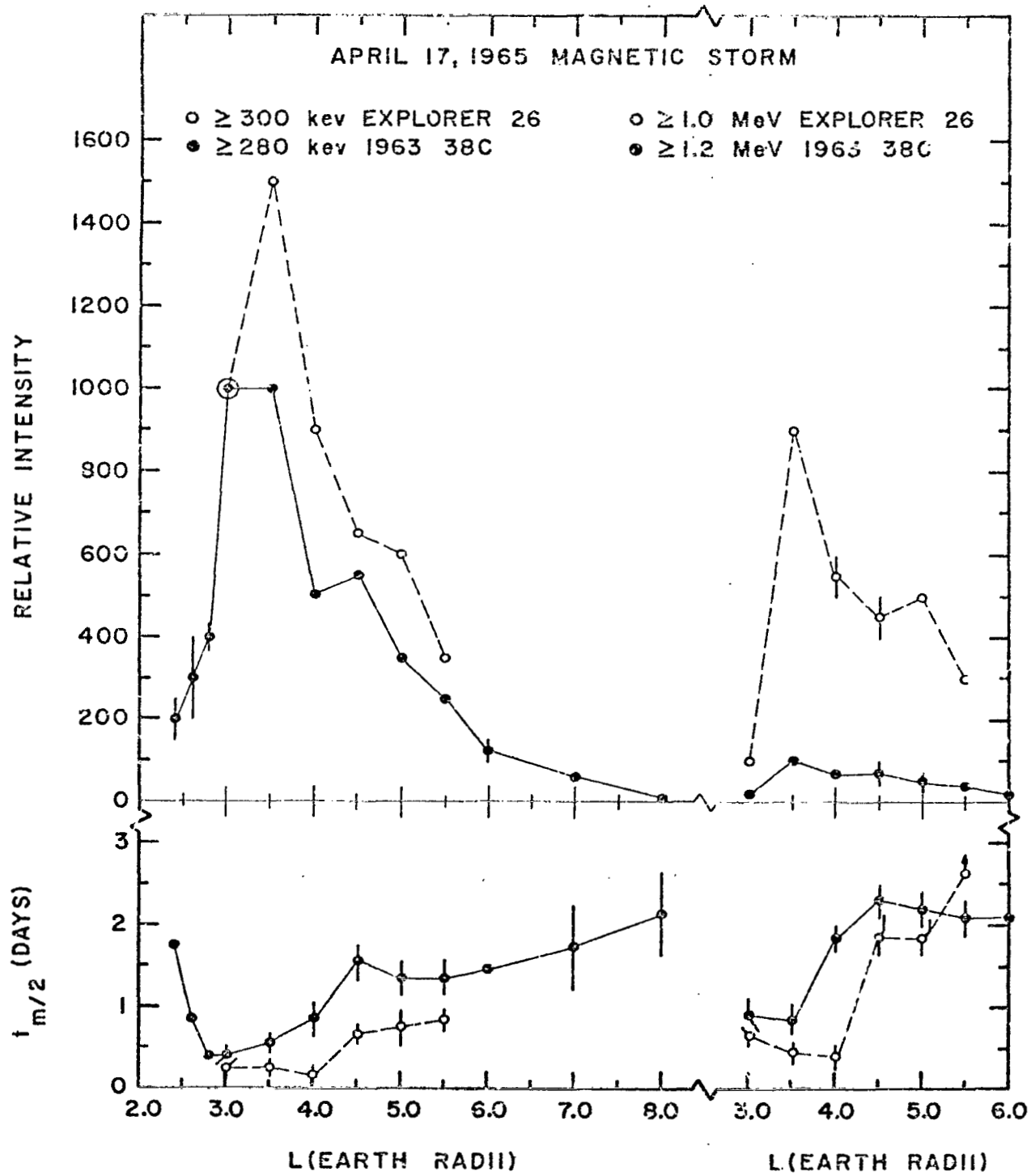
APRIL 17, 1965 MAGNETIC STORM
○ ≥ 300 kev EXPLORER 26
● ≥ 280 kev 1963 38C
○ ≥ 1.0 MeV EXPLORER 26
● ≥ 1.2 MeV 1963 38C
RELATIVE INTENSITY
1600
1400
1200
1000
800
600
400
200
0
$t_{m/2}$ (DAYS)
3
2
1
0
2.0
3.0
4.0
5.0
6.0
7.0
8.0
3.0
4.0
5.0
6.0
L(EARTH RADII)
L(EARTH RADII)

Figure 11

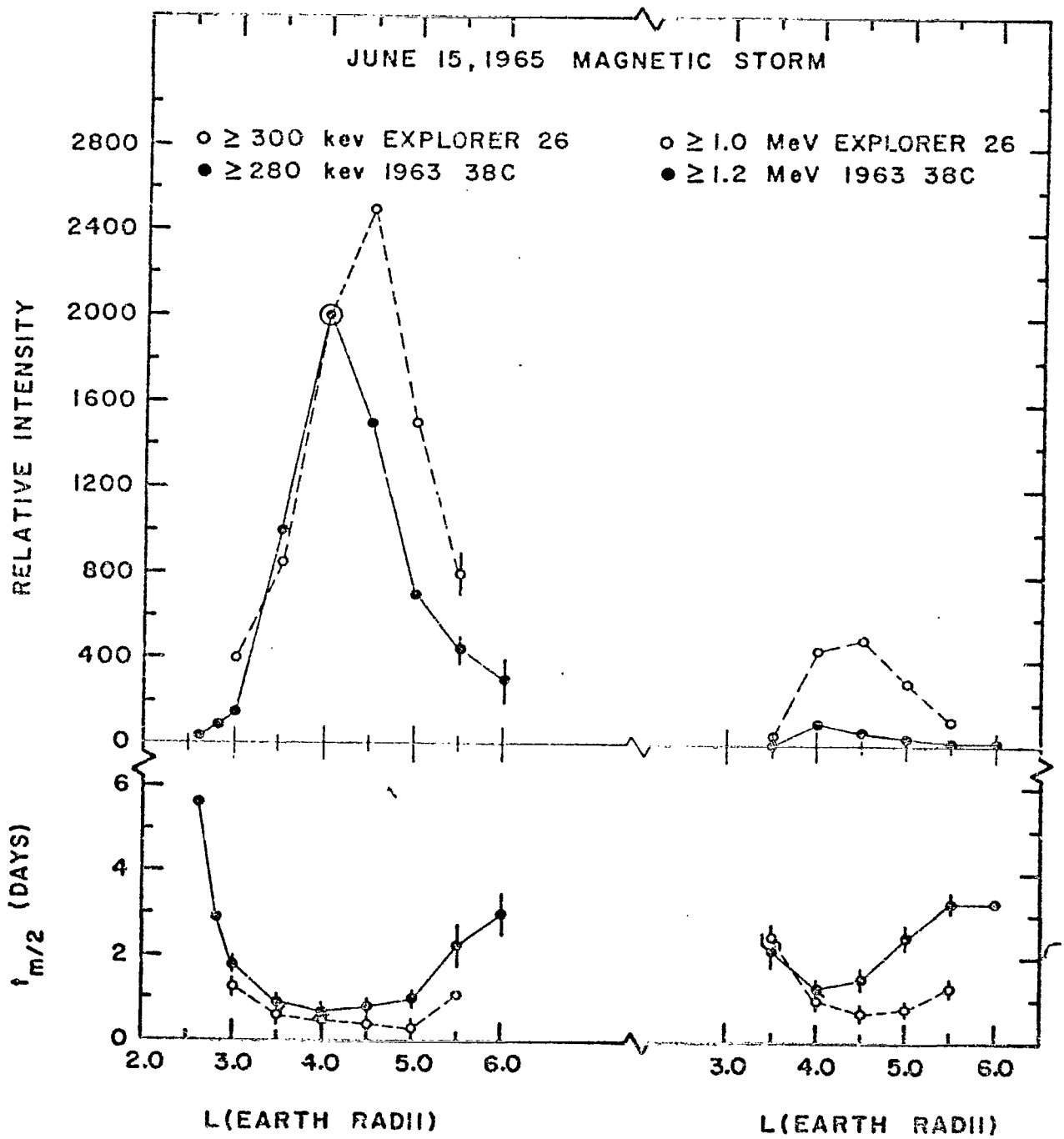
JUNE 15, 1965 MAGNETIC STORM
o ≥ 300 kev EXPLORER 26
● ≥ 280 kev 1963 38C
o ≥ 1.0 MeV EXPLORER 26
● ≥ 1.2 MeV 1963 38C
RELATIVE INTENSITY
2800
2400
2000
1600
1200
800
400
0
$t_{m/2}$ (DAYS)
6
4
2
0
2.0
3.0
4.0
5.0
6.0
L(EARTH RADII)
3.0
4.0
5.0
6.0
L(EARTH RADII)

Figure 12

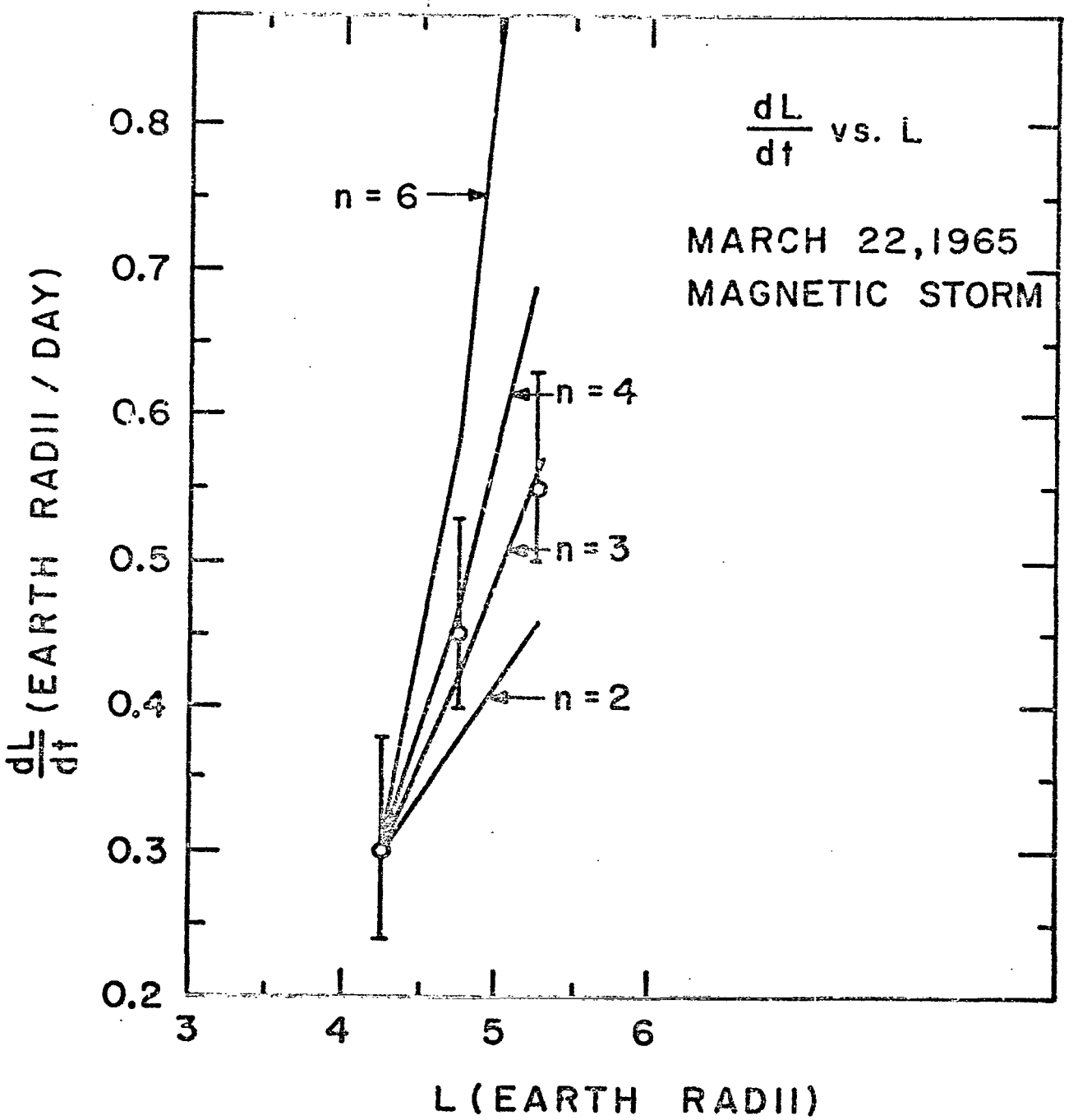
dL/dt vs. L
MARCH 22, 1965
MAGNETIC STORM
n = 6
n = 4
n = 3
n = 2
dL/dt (EARTH RADII / DAY)
0.8
0.7
0.6
0.5
0.4
0.3
0.2
3
4
5
6
L (EARTH RADII)

Figure 13

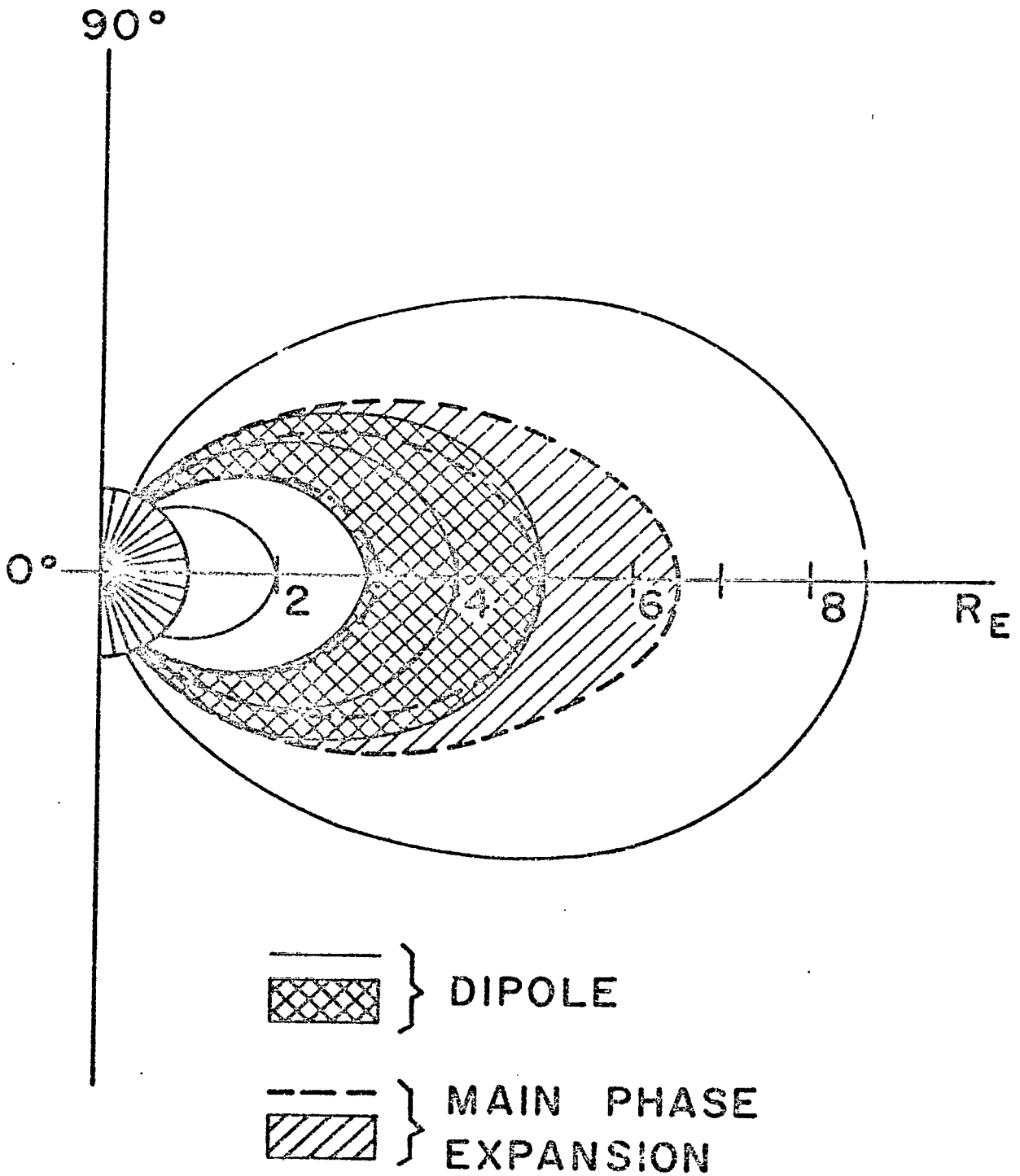


Figure 14

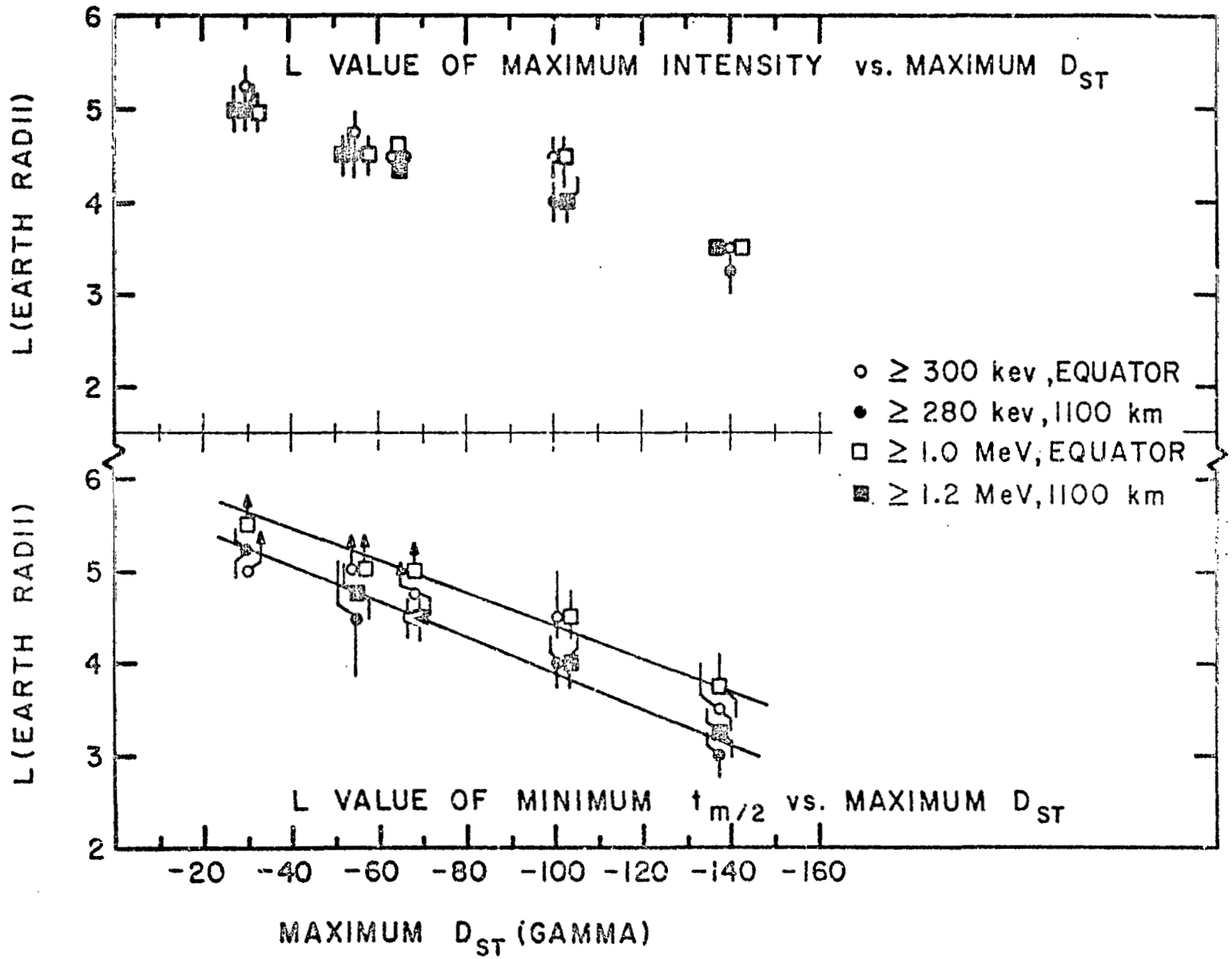
L VALUE OF MAXIMUM INTENSITY vs. MAXIMUM $D_{ST}$
L(EARTH RADII)
6
5
4
3
2
○ ≥ 300 kev, EQUATOR
● ≥ 280 kev, 1100 km
□ ≥ 1.0 MeV, EQUATOR
■ ≥ 1.2 MeV, 1100 km
L VALUE OF MINIMUM $t_{m/2}$ vs. MAXIMUM $D_{ST}$
-20 -40 -60 -80 -100 -120 -140 -160
MAXIMUM $D_{ST}$ (GAMMA)

Figure 15

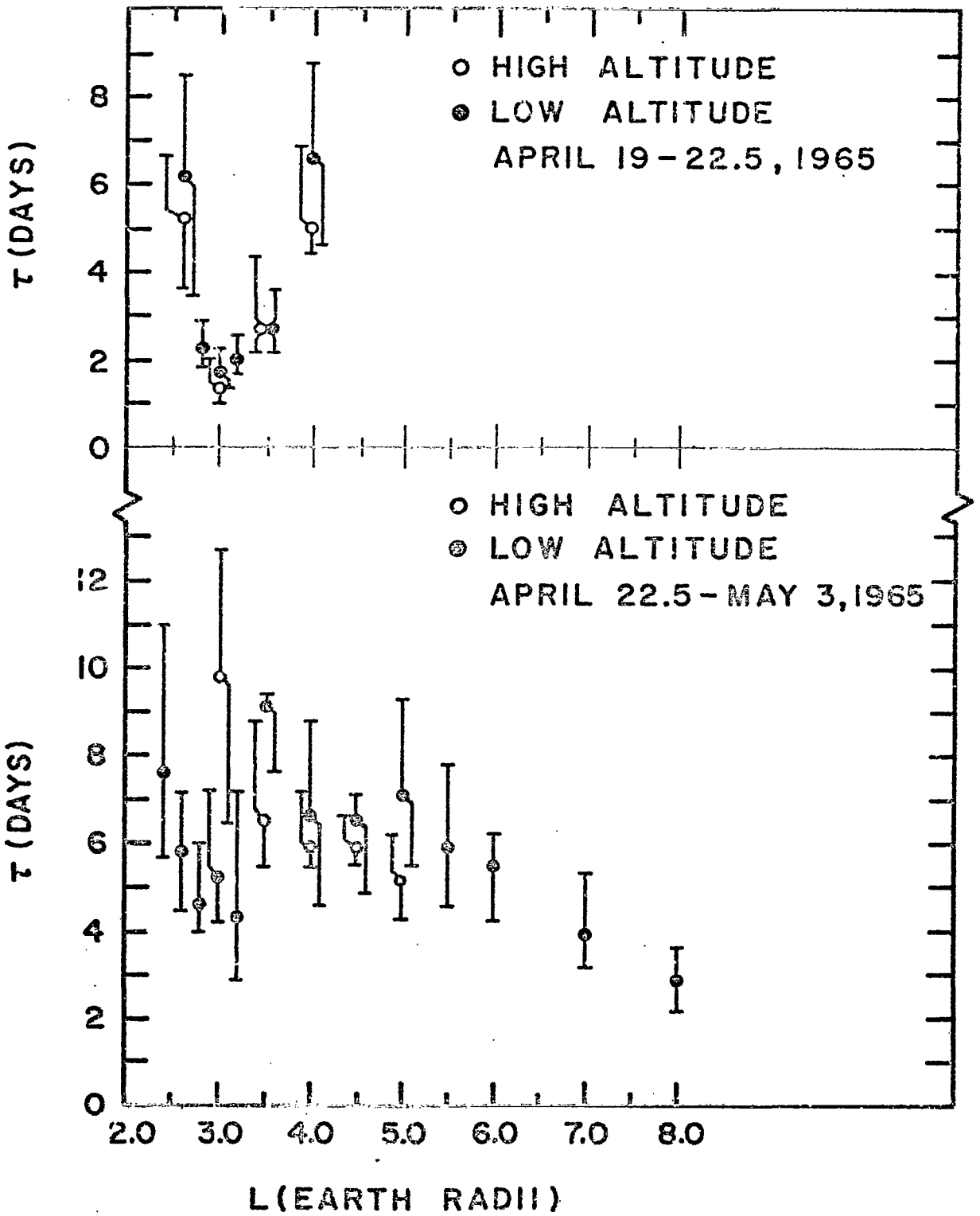
o HIGH ALTITUDE
● LOW ALTITUDE
APRIL 19 - 22.5, 1965
τ (DAYS)
0
2
4
6
8
o HIGH ALTITUDE
● LOW ALTITUDE
APRIL 22.5 - MAY 3, 1965
τ (DAYS)
0
2
4
6
8
10
12
2.0
3.0
4.0
5.0
6.0
7.0
8.0
L (EARTH RADII)

Figure 16

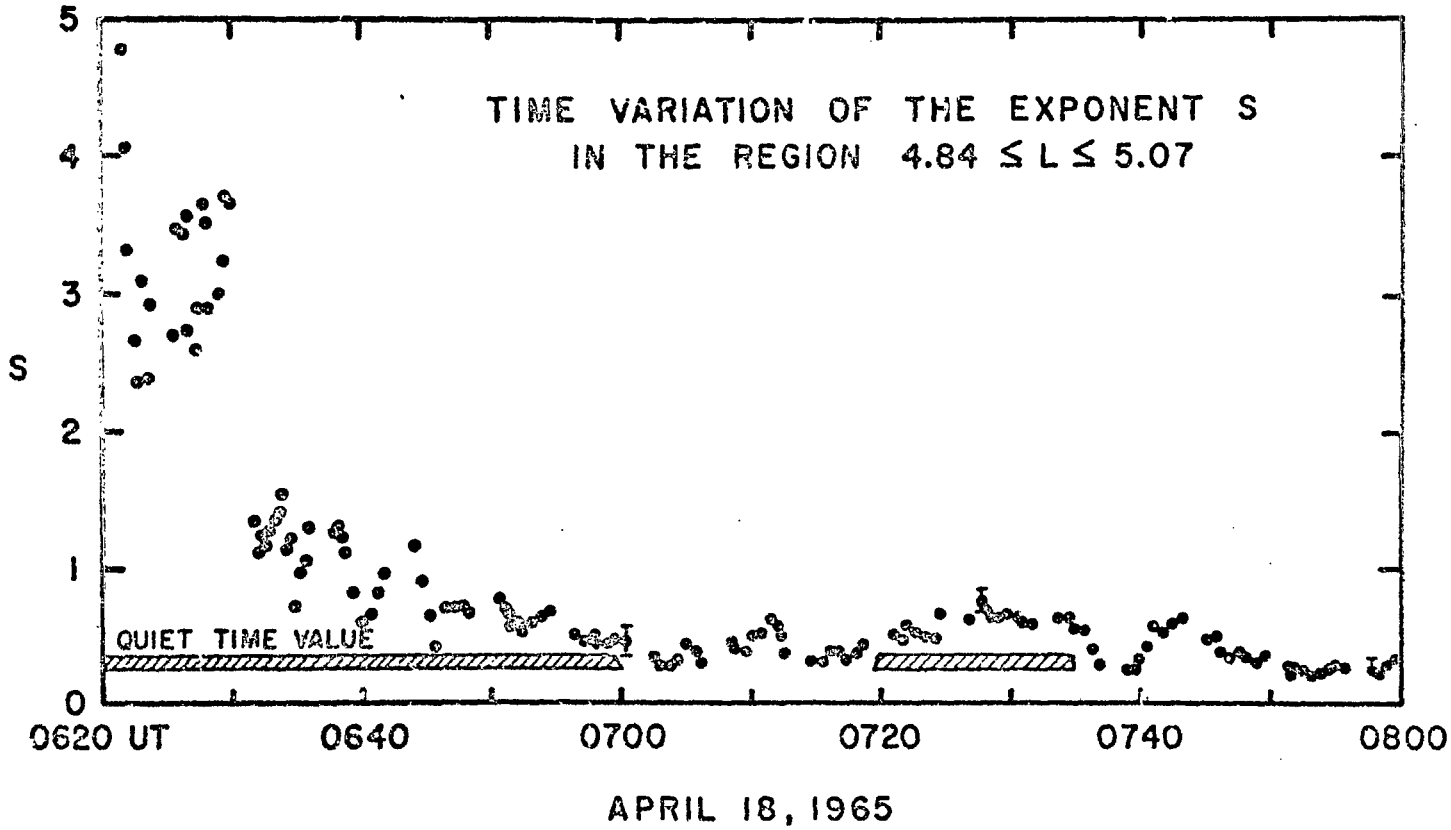
TIME VARIATION OF THE EXPONENT S
IN THE REGION 4.84 ≤ L ≤ 5.07
S
5
4
3
2
1
0
QUIET TIME VALUE
0620 UT
0640
0700
0720
0740
0800
APRIL 18, 1965

Figure 17

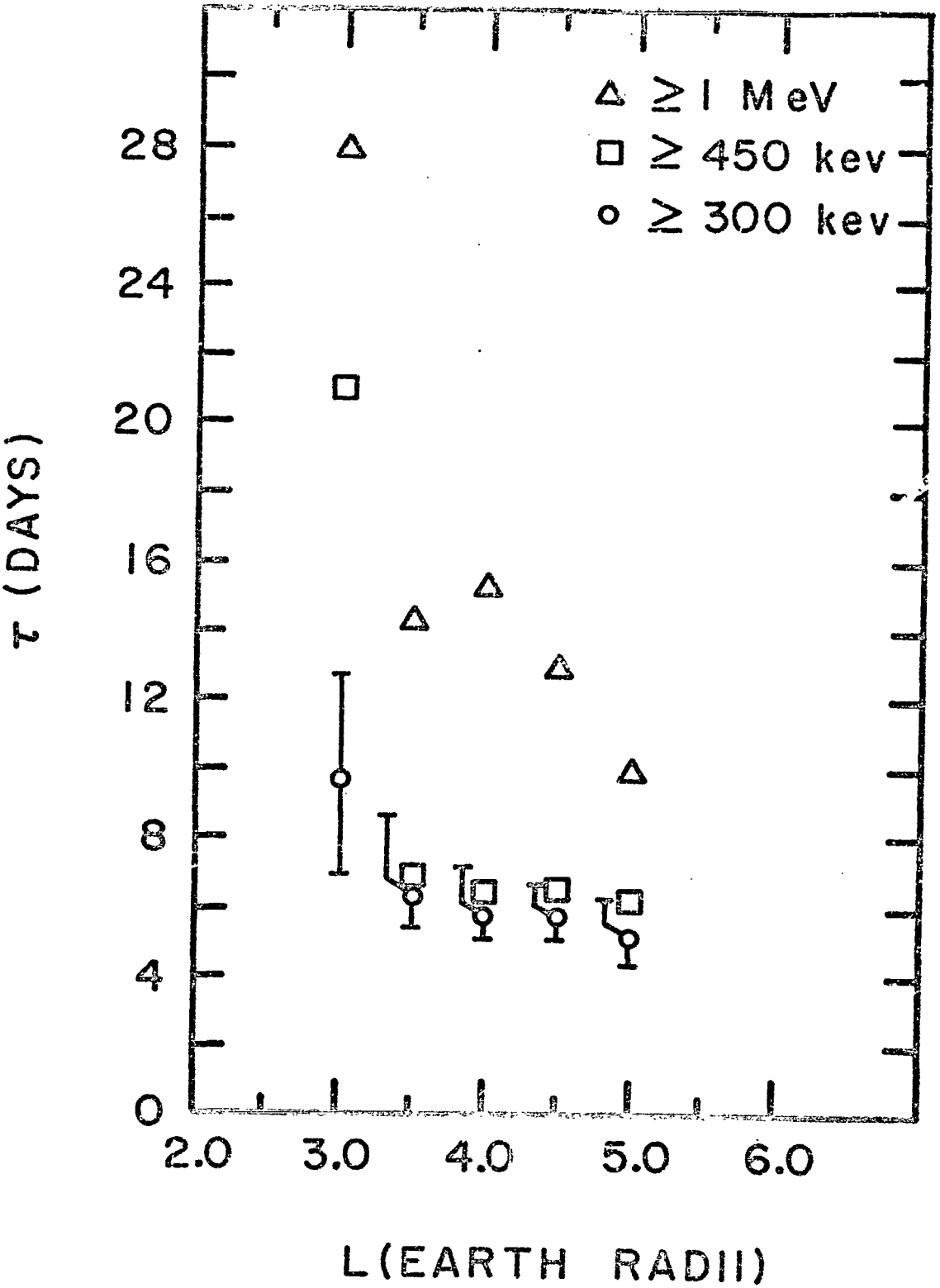
Δ ≥ 1 MeV
□ ≥ 450 kev
o ≥ 300 kev
τ (DAYS)
0
4
8
12
16
20
24
28
2.0
3.0
4.0
5.0
6.0
L(EARTH RADII)

Figure 18

REFERENCES


Arens, J. F., and D. J. Williams, "Long Term Time History of Outer Zone Trapped Electrons at 1100 km," (abstract) Trans. Am. Geophys. Union, 48, 169, 1967.

Arens, J. F., D. J. Williams, L. J. Lanzerotti, and C. S. Roberts, "Comparison of Outer Zone Trapped Electron Behavior at 1100 km and at 3-5 $R_E$ during the April 18, 1965, Magnetic Storm," Trans. Am. Geophys. Union, 48, 169, 1967.

Bauer, S. J., and B. V. Krishnamurthy, "Possible Relationship Between the Stormtime Whistler Cutoff and the Magnetospheric Ring Current," J. Geophys Res., 73, March 1, 1968a.

Bauer, S. J., and B. V. Krishnamurthy, "Behavior of the Topside Ionosphere During a Great Magnetic Storm," Planet. Space Sci., 1968b.

Block, L. P., "On the Distribution of Electric Fields in the Magnetosphere," J. Geophys. Res., 21, 855-864, 1966.

Bostrom, C. O., J. W. Kohl, and D. J. Williams, "The February 5, 1965, Solar Proton Event, 1, Time History and Spectrums Observed at 1100 km," J. Geophys. Res., 72, 4487-4495, 1967.

Brown, W. L., and C. S. Roberts, "Observations of Outer Zone Electrons on April 18, 1965, by the Explorer 26 Satellite," (abstract) Trans. Am. Geophys. Union, 47, 135, 1966.

Buck, T. M., G. H. Wheatley, and J. W. Rodgers, "Silicon p-n Junction Radiation Detectors for the Telstar Satellite," IEEE Trans. Nuc. Sci., NS-11, 294-301, 1964.

Cahill, L. J., Jr., "Inflation of the Inner Magnetosphere During a Magnetic Storm," J. Geophys. Res., 71, 4505-4519, 1966.

Carpenter, D. L., "Whistler Evidence of a 'knee' in the Magnetospheric Ionization Density Profile," J. Geophys. Res., 68, 1675-1682, 1963.

Carpenter, D. L., "Whistler Studies of the Plasmapause in the Magnetosphere 1. Temporal Variations in the Position of the Knee and some Evidence on Plasma Motions near the Knee," J. Geophys. Res., 71, 693-709, 1966.

Craven, J. D., "Temporal Variations of Electron Intensities," J. Geophys. Res., 71, 5643-5664, 1966.

Fälthammer, C-G., "Effects of Time-Dependent Electric Fields on Geomagnetically Trapped Radiation," J. Geophys. Res., 70, 2503-2516, 1965.

Forbusch, S. E., G. Pizzella, and D. Venkatesan, "The Morphology and Temporal Variations of the Van Allen Radiation Belt, October 1959 to December 1960," J. Geophys. Res., 67, 3651-3668, 1962.

Frank, L. A., "A Survey of Electrons E > 40 kev Beyond 5 Earth Radii with Explorer 14," J. Geophys. Res., 70, 1593-1626, 1965a.

Frank, L. A., "Inward Radial Diffusion of Electrons Greater the 1.6 Million Electron Volts in the Outer Radiation Zone," J. Geophys. Res., 70, 3533-3540, 1965b.

Frank, L. A., "On the Extraterrestrial Ring Current During Geomagnetic Storms," J. Geophys. Res., 72, 3753-3767, 1967.

Hoffman, R. A., and P. Bracken, "Magnetic Effects of the Quiet Time Proton Belt," J. Geophys. Res.,70, 3541-3556, 1965.

Kennel, C. F., and H. E. Petschek, "Limit on Stably Trapped Particle Fluxes," J. Geophys. Res., 71, 1-28, 1966.

Lanzerotti, L. J., "Outer Zone Electron Fluxes During the February 5, 1965, Solar Proton Event," Annals de Geophysique, 1968, to be published.

Lincoln, J. V., "Geomagnetic and Solar Data," J. Geophys. Res., 70, 5953-5955, 1965.

Lincoln, J. V., "Geomagnetic and Solar Data," J. Geophys. Res., 71, 1477-1479, 1966.

McDiarmid, I. B., and J. R. Burrows, "Dependence of the Position of the Outer Radiation Zone Intensity Maxima on Electron Energy and Magnetic Activity," Can. Journal of Physics, 45, 2873-2878, 1967.

Nakada, M. P., and G. D. Mead, "Diffusion of Protons in the Outer Radiation Belt," J. Geophys. Res., 70, 4777-4791, 1965.

O'Brien, B. J., "A Large Diurnal Variation of the Geomagnetically Trapped Radiation," J. Geophys. Res., 68, 989-996, 1963.

O'Brien, B. J., "High-Latitude Geophysical Studies with Satellite Injun 3, 3: Precipitation of Electrons into the Atmosphere," J. Geophys. Res., 69, 13-43, 1964.

Parker, E. N., "Geomagnetic Fluctuations and the Form of the Outer Zone of the Van Allen Radiation Belt," J. Geophys. Res., 65, 3117-3130, 1960.

Roberts, C. S., "On the Relationship Between the Unidirectional and Omnidirectional Flux of Trapped Particles on a Magnetic Line of Force," J. Geophys. Res., 70, 2517-2527, 1965.

Roberts, C. S., "Electron Loss from the Van Allen Zones due to Pitch Angle Scattering by Electromagnetic Disturbances," in Proc. Advanced Study Institute, Radiation Trapped in the Earth's Magnetic Field, edited by B. M. McCormac, 151-168, D. Reidel Publishing Co., 1966.

Roberts, C. S., "Cyclotron Resonance and Bounce Resonance Scattering of Electrons Trapped in the Earth's Magnetic Field," Earth's Particles and Fields, edited by B. M. McCormac, Reinhold Publishing Corp., 1968.

Rose, D. C., "The Alouette Satellite Results," in Proc. Advanced Study Institute, Radiation Trapped in the Earth's Magnetic Field, edited by B. M. McCormac, 191-213, D. Reidel Publishing Co., 1966.

Sugiura, M., and S. Hendricks, "Provisional Hourly Values of Equatorial $D_{st}$ for 1961, 1962, and 1963," NASA/GSFC Document X-612-66-355, August, 1966.

Tverskoy, B. A., "Dynamics of the Radiation Belts of the Earth, 2," Geomagnetism and Aeronomy, 3, 351-366, 1964.

Williams, D. J., and A. M. Smith, "Daytime Trapped Electron Intensities at High Latitudes at 1100 kilometers," J. Geophys. Res., 70, 541-556, 1965.

Williams, D. J., "Outer Zone Electrons," in Proc. Advanced Study Institute, Radiation Trapped in The Earth's Magnetic Field, edited by B. M. McCormac, 263-280, D. Reidel Publishing Co., 1

END

DATE

FILMED

APR 8 1968